ELSEVIER

Coordination Chemistry Reviews 230 (2002) 171–192

COORDINATION CHEMISTRY REVIEWS

www.elsevier.com/locate/ccr

Transition metal based supramolecular systems: synthesis, photophysics, photochemistry and their potential applications as luminescent anion chemosensors

Shih-Sheng Sun, Alistair J. Lees *

Department of Chemistry, State University of New York at Binghamton, Binghamton, NY 13902-6016, USA

Received 11 July 2001; accepted 8 February 2002

Dedicated to Professor Derk J. Stufkens and his outstanding contributions to organometallic photophysics and photochemistry

Contents

Abstract . . . 171
1. Introduction . . . 172
2. Self-assembly triangular and square rhenium(I) tricarbonyl complexes . . . 173
   2.1 Preparation of self-assembly homometallic molecular squares and triangles . . . 173
   2.2 Photophysical properties . . . 173
   2.3 Host–guest interactions . . . 176
3. Self-assembly organometallic squares with terpyridyl metal complexes as bridging ligands . . . 177
   3.1 Preparation of self-assembly octanuclear molecular squares linked by a metal-complex ligand . . . 177
   3.2 Photophysical properties . . . 177
   3.3 Host–guest interactions . . . 178
4. Self-assembly organometallic molecular cages comprising of 11 components . . . 180
   4.1 Preparation of self-assembly molecular cages . . . 181
   4.2 Photophysical properties . . . 181
   4.3 Host–guest interactions . . . 182
5. Photoswitchable trinuclear *fac*-(diimine)Re(I)$(CO)_3$ complexes linked by a stilbene-like bridging ligand . . . 183
   5.1 Synthesis . . . 183
   5.2 Photophysical properties and photoinduced isomerization . . . 183
6. Complexes exhibiting luminescent anion receptor behavior via hydrogen bonding . . . 185
   6.1 Synthesis and physical properties . . . 186
   6.2 Anion sensing studies . . . 186
7. Dinuclear metal complexes bridged by macrocyclic phenylacetylenic ligands . . . 187
   7.1 Synthesis . . . 188
   7.2 Photophysical properties . . . 189
8. Concluding remarks . . . 190
Acknowledgements . . . 190
References . . . 190

Abstract

This review describes our recent research results on several transition-metal based supramolecular systems. A number of self-assembly metallocyclophanes and cages have been prepared. We have found that the photophysical properties of these systems are highly dependent on the nature of the bridging ligands and that many of these metallocyclophanes and cages are capable of binding

* Corresponding author. Tel.: +1-607-777-2362; fax: +1-607-777-4478
E-mail address: alees@binghamton.edu (A.J. Lees).

0010-8545/02/$ - see front matter
PII: S0010-8545(02)00043-7

different guest molecules such as inorganic anions and a variety of aromatic compounds. Moreover, trinuclear (diimine) rhenium(I) tricarbonyl complexes linked by a stilbene-like ligand exhibit most interesting photoswitching features, where the luminescence from the complexes can be switched on and off by photoinduced ligand isomerization. In addition, a structurally simple and easily synthesized luminescent anion receptor has been recently developed and it displays outstanding sensitivity and selectivity toward anionic species. We also review the synthesis of two shape-persistent hexagonal phenylacetylenes and their use as ligands to synthesize dinuclear transition-metal complexes. The photophysical properties of both phenylacetylenic ligands and their corresponding metal complexes are summarized.

Keywords: Supramolecular chemistry; Self assembly; Transition-metal organometallic complexes; Metallocyclophanes; Host–guest systems; Photoinduced energy transfer; Molecular switches; Luminescence sensors; Photophysical processes; Photochemistry; Macrocyclic ligands

1. Introduction

Luminescent polynuclear transition-metal complexes containing multichromophoric ligands with extended conjugation have been extensively studied in recent years, partly because of their potential use as sensors, probes, and photonic devices [1]. Among numerous luminescent transition-metal complexes, Re(I)-, Ru(II)- and Os(II)-based polypyridyl chromophores are the most commonly studied because they usually exhibit fairly strong luminescence in the visible region and the photophysical properties are relatively easily tuned by simply modifying the coordinated or ancillary ligands [2]. These compounds also have the advantage of being relatively stable with respect to photodecomposition. In each case, the emission from the complexes usually originates from triplet metal-to-ligand charge transfer (^{3}MLCT) excited states and has the added feature of being typically sensitive to the nature of the environment and influenced by solvent, temperature, and pH [3,4]. The pioneering work by Stufkens et al. on the nature and reactivity of organometallic excited states has laid the foundation for much of these studies [5–8].

During the last decade, research on transition metal mediated self-assembled supramolecular entities has experienced extraordinary progress [9–15]. In terms of bonding strength, the relatively weak coordination bonds formed to transition metals lie intermediate between the strong covalent bonding in carbon-based systems and the weak interactions of biological systems. Some of the advantages of employing transition metals to build self-assembly supramolecular complexes include, (1) the involvement of d orbitals which offer more bonding modes and geometrical symmetries than simple organic molecules; (2) a range of electronic and steric properties that can be fine-tuned by employing different ancillary ligands; (3) the ability to easily modify the size of the desired supramolecules by utilizing different lengths of bridging ligands; and (4) the incorporation of their distinct spectral, magnetic, redox, photophysical and photochemical properties. Moreover, the diverse bonding angles imparted by the transition metal centers and the high directionality of the dative bonding between the ligands and metals also provide superior features over other weak intermolecular interactions, such as electrostatic, van der Waals, and π–π interactions. Another interesting aspect is that thermodynamically-driven spontaneous self-assembly of individual molecular components into well-defined molecular structures in solution is expected to be rather similar for both coordination chemistry and biology and this enables transition-metal complexes to be valuable mimics of the more complicated biological systems [16].

We have been interested in the photophysical and excited state properties of polynuclear rhenium(I) tricarbonyl complexes linked by polypyridyl ligands. The thermally labile nature of the rhenium(I) tricarbonyl moiety has been proved to be a valuable component to construct self-assembly metallocyclophanes [17]. Our recent studies have focused on synthesizing a variety of rhenium(I) tricarbonyl based self-assembly metallocyclophanes or cages as well as some polynuclear rhenium(I) tricarbonyl complexes [18–25]. These various systems have illustrated many interesting new chemical and physical properties, particularly in the areas of structural diversity, excited state dynamics, electrochemistry, photoswitching, molecular recognition, and anion sensing. Herein, we review some of our recent results and focus on four different aspects, (a) new self-assembly metallocyclophanes and cages [18–22]; (b) systems that exhibit photoinduced luminescence switching [23]; (c) complexes that display luminescent anion recognition properties via hydrogen bonding interaction [24]; and (d) novel dinuclear metal complexes bridged by macrocyclic phenylacetylenic ligands [25].

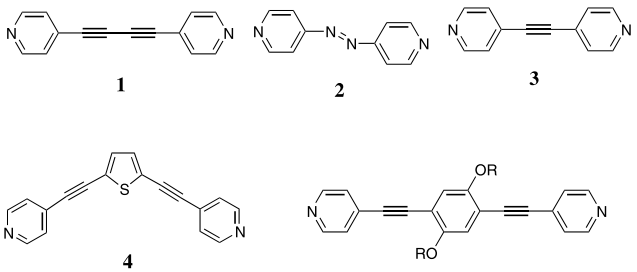

Chart 1.

2. Self-assembly triangular and square rhenium(I) tricarbonyl complexes

2.1. Preparation of self-assembly homometallic molecular squares and triangles

Hupp and coworkers prepared the first self-assembly molecular squares utilizing octahedral rhenium(I) carbonyl centers in 1995 [26]. The incorporation of potentially luminescent *fac*-tricarbonyl Re(I) diimine chromophores into the macrocyclic structures offers rich photophysical properties and potential applications as sensors or ultrafine sieves [27]. We have prepared a series of homometallic molecular triangles and squares assembled from $XRe(CO)_5$ (X = Cl or Br) and a variety of bipyridyl ligands [18,19]. The structures of the bridging ligands are shown in Chart 1. We have found that the disposition of the binding sites and the length of the bridging ligands greatly influence the final self-assembly architectures. Thus, a molecular square can be assembled from a bis-monodentate ligand with a 180° binding angle with $ClRe(CO)_5$ (see Scheme 1), while a bridging ligand with a roughly 120° binding angle forms dinuclear macrocycle with $ClRe(CO)_5$, and a slightly less thermodynamically stable trinuclear pseudohexagon is also formed during the early stage of the reaction (see Scheme 2). Interestingly, only molecular triangles were isolated when employing longer bridging ligands (see Scheme 3). The fact that the molecular triangle appears as the only product without formation of the molecular square implies that the entropy effect plays a more important role than the enthalpy effect in the self-assembly process.

2.2. Photophysical properties

Table 1 summarizes the photophysical data of complexes **7**–**13** as well as their corresponding bridging ligands **1**–**6** and corner complexes **14**–**16** (see Chart 2 for their structures). The electronic absorption spectra of all the compounds exhibit two main features that are assigned as bridging-ligand-localized $\pi \rightarrow \pi^*$ and metal-to-bridging-ligand charge transfer (MLCT) transitions. In squares **7** and **9**, the lowest-energy band is solely of MLCT character, while in compounds **8**, **10**, **12**, and **13**, the $\pi \rightarrow \pi^*$ and MLCT bands are substantially overlapping. Square **8** exhibits an additional low-energy $n \rightarrow \pi^*$ transition that originates from the *trans*-AZP ligand which substantially overlaps with the MLCT band. Significantly, we find that the character of the lowest-energy bands has a profound influence on the observed photophysical and photochemical properties.

Fig. 1 compares the absorption spectra of square **7**, corner **14**, and ligand **1**, in THF solution. It is very clear from the vibronic structure of the high-energy bands below 320 nm that these bands originate from ligand localized $\pi \rightarrow \pi^*$ transitions. The lowest energy bands in square **7** and corner **14** are assigned to MLCT transitions. The MLCT band in square **7** red shifts 1385 cm^{-1} compared with that of the corner **14**. A similar red shift has also been observed from the protonated corner of *fac*-$ClRe(CO)_3(4,4'\text{-bpy})_2$ by Giordano and Wrighton [28]. This result can be ascribed to either the fact that there is a more extended conjugation in square **7** than in corner **14** or the influence of the electrostatically stabilizing negative charge in the ligand π^* orbital by Re(I) [23,28,29].

Square **7** exhibits luminescence at room temperature (r.t.), which is independent of the excitation wavelength (340–400 nm), with an emission lifetime of 39 ns in THF solution. The wavelength-independent emission spectrum and the good congruence between the absorption and excitation spectra of square **7** indicate that the internal conversion from higher excited states to the lowest ^{3}MLCT state is highly efficient and that luminescence originates solely from the lowest ^{3}MLCT state. The assignment of the lowest-emitting level as MLCT in character is based on the position and shape of the emission band and the emission lifetime which are consistent with those previously reported for similar complexes assigned as MLCT emitters [23,28–31]. As observed in the absorption spectra, the emission maxima

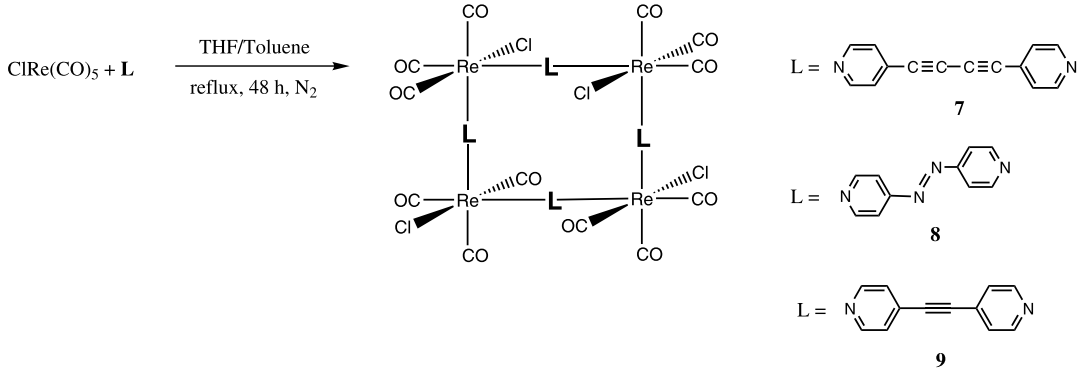

Scheme 1.

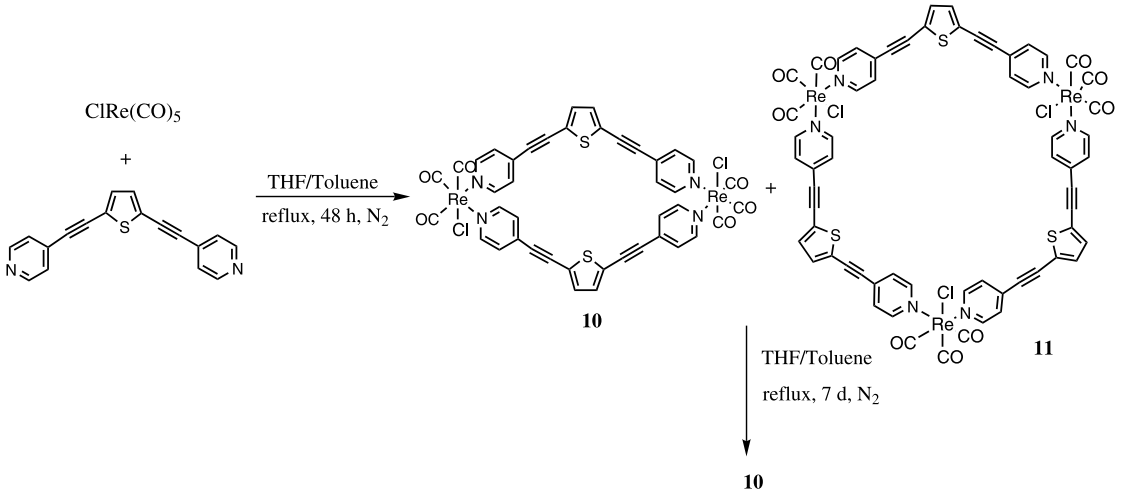

Scheme 2.

of square **7** shift to lower energy compared with the emission maxima of its corner **14**. The emission lifetime of square **7** is shorter than its corner **14**; this is attributed to an enhanced nonradiative decay rate for square **7** due to the lower energy of the excited state with a more effective vibronic overlap [28–30].

In contrast, neither square **8** nor its corner **15** have any detectable luminescence in r.t. under the same experimental conditions. This is attributed to effective intramolecular energy transfer from the initially formed ^{1,3}MLCT excited states to the lowest non-emitting $n \rightarrow \pi^*$ state [32].

The absorption spectrum of the dinuclear macrocycle **10** features a broad band centered at 383 nm and a shoulder at 422 nm. The low energy shoulder is assigned to be MLCT in character and the band at 383 nm is assigned to a ligand localized $\pi \rightarrow \pi^*$ transition. In contrast to its free ligand **4**, which exhibited strong fluorescence in r.t. CH_2Cl_2 solution, there is no luminescence detected from **10** in r.t. CH_2Cl_2 solution. The lack of emission can also be attributed to the efficient vibrational relaxation on the basis of the energy gap law [30].

The detailed photophysical data of **12** and **13** are summarized in Table 1. In general, the photophysical properties of triangles **12** and **13** are very similar. The following discussion will mainly focus on triangle **12**, but will point out any notable differences in the physical properties of **13**. The absorption spectrum of **12** differs significantly in comparison to its corresponding free bridging ligand **5**. The spectrum of **12** exhibits two broad bands and both bands are red-shifted compared with the absorption bands of **5**. The intensity ratio of the lower energy band vs. the higher energy band is also larger in **12** than the corresponding ratio in **5**. The lowest energy band is assigned to a mixture of MLCT and $\pi \rightarrow \pi^*$ excited states. The r.t. emission spectrum of **12** in $ClCH_2CH_2Cl$ exhibits structured features with maxima at 499 and 476 nm. It should be noted that the luminescence is not dependent on the excitation wavelength in the 340–400 nm range and that there is a single exponential decay from these two bands. The low-

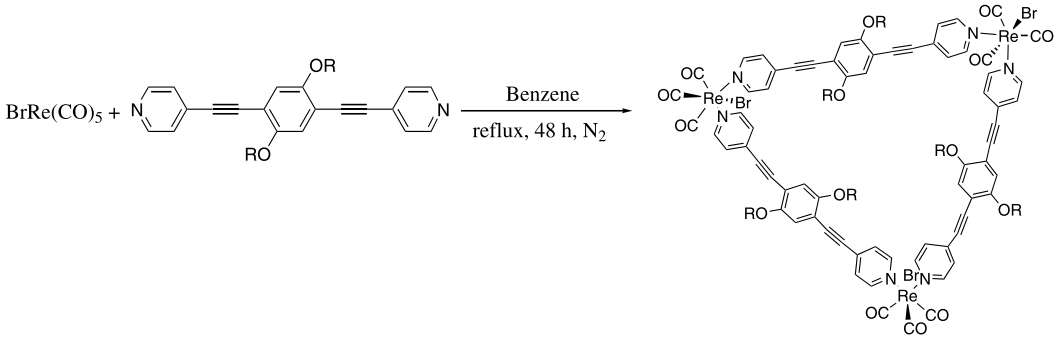

Scheme 3.

Table 1
Electronic absorption and emission data of metallocyclophanes and their associated free ligands and corner complexes at 293 K

Compounds	Absorption spectra	Emission		
	λ_{max}, nm (10^{-3} ε, M^{-1} cm^{-1})	λ_{max}, nm	τ, ns	Φ_{em}
7 [a]	256 (227), 298 (141), 322 (151), 360 (160)	635	39	8.5×10^{-4}
8 [b]	272 (243), 391 (123)	[c]		
9 [d,e]	263 (sh), 281, 292, 355	622	82	0.0021
10 [d]	383 (107), 422 (46.8)	[c]		
12 [f]	329 (118), 406 (145)	499, 476	0.36	0.032
13 [f]	243 (86.4), 261 (71.6), 329 (113), 412 (142)	512, 470	0.37	0.012
14 [a]	250 (64.1), 287 (37.8), 301 (42.4), 320 (46.0), 342 (38.3)	600	110	0.011
15 [b]	282 (56.8), 355 (22.9)	[c]		
16 [d]	281 (41.7), 296 (38.3), 326 (20.0)	592	160	0.0083
1 [a]	244 (18.9), 253 (17.8), 272 (8.1), 284 (11.9), 302 (15.2), 323 (13.2)	[c]		
2 [d]	287 (19.9), 458 (0.24)	[c]		
3 [d]	263 (sh, 15.5), 275 (20.3), 290 (15.3)	[c]		
4 [d]	248 (14.6), 266 (13.2), 351 (47.7), 372 (sh, 36.2)	404, 384	0.26	0.26
5 [f]	308 (12.0), 318 (11.5), 377 (9.5)	450 (sh), 427	2.5	0.59
6 [f]	308 (12.6), 318 (13.7), 340 (sh, 7.9), 388 (10.1)	446, 426	2.6	0.30

Data taken from Refs. [14,15].
[a] THF solution, $\lambda_{ex} = 400$ nm.
[b] DMF solution.
[c] No detectable emission in r.t. solution.
[d] CH_2Cl_2 solution, $\lambda_{ex} = 360$ nm.
[e] The solubility is too low to accurately determine the extinction coefficient.
[f] $ClCH_2CH_2Cl$ solution, $\lambda_{ex} = 360$ nm.

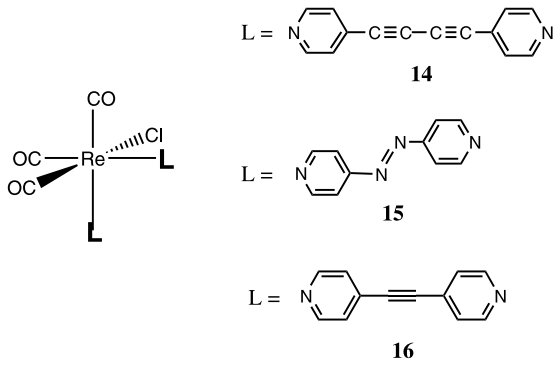

Chart 2.

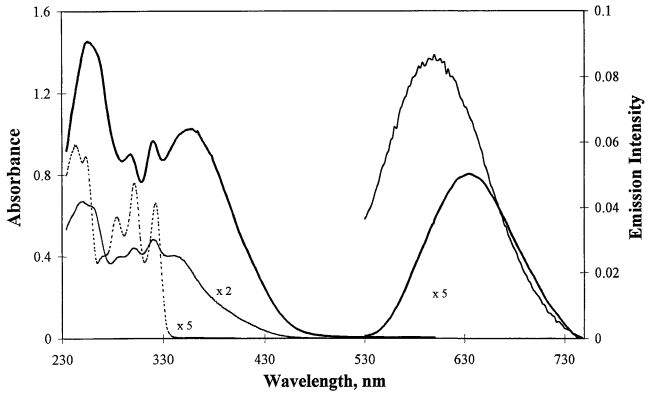

Fig. 1. Electronic absorption and emission spectra of 7.5×10^{-6} M square **7** (▬), corner **14** (—), and ligand **1** (---) in THF at 293 K. Reprinted, with permission, from Ref. [19].

temperature (77 K) emission spectrum of **12** in 2-methyltetrahydrofuran displays more distinct structure with bands at 463, 488, 520 and 549 nm (1188 cm^{-1} average spacing). These observations illustrate that the dual emission bands are actually vibronic structure from the π–π* excited state. The very small blue shift on going from the solution to a rigid glass also supports the assignment of the emission from a ligand-based π→π* excited state [3,33].

Careful scrutiny of the photophysical data of triangle **12** and its free ligand **5** reveals several interesting points. The extremely short lifetime and relatively high-energy emission from **12** indicate that the emission is apparently ligand-localized ^{1}π–π* fluorescence. Fluorescence from the ^{1}π–π* state is typically not observed in transition metal complexes [3]. However, the fast radiative decay rate ($k_r \sim 10^8$ s^{-1}) from the ^{1}π–π* excited state localized on **5** indicates that the fluorescence is still able to compete with the other nonradiative deactivation processes. In addition, **5** exhibits a longer lifetime than **12** and the quantum yield of **5** is almost 20 times larger than in **12**. On this basis, it can be concluded that the $Re(CO)_3Br$ moieties in **12** act as energy quenchers. Consequently, the relatively low fluorescence quantum yield and short lifetime in r.t. solution are due to the effective intramolecular energy transfer from the ^{1}π–π* state to the ^{3}MLCT or ^{3}π–π* states [34–36]. Considering the large spin-orbital coupling exerted from Re(I) atoms [3], it is anticipated that there ought to be emission observed from either the ^{3}MLCT or ^{3}π–π*

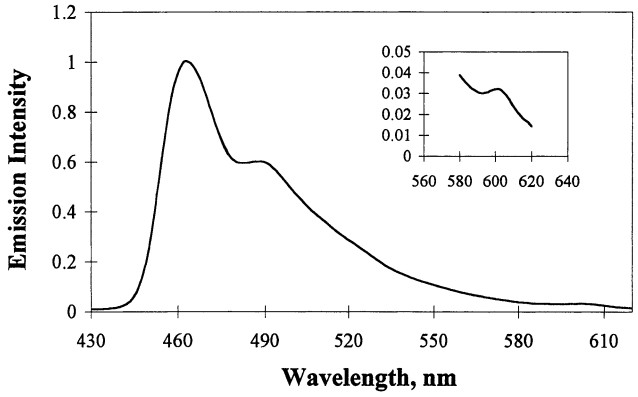

Fig. 2. Emission spectrum of triangle **12** in a 77 K 2-methyltetrahydrofuran glass. The inset shows the lowest-energy band. Reprinted, with permission, from Ref. [19].

excited states in triangle **12**. The folding motions of the hexyloxyl chains in **12** are believed to be responsible for the rapid vibrational relaxation from the ^{3}MLCT excited state. This is further supported by the higher quantum yield of **5** and its corresponding triangle in comparison to **6** and its corresponding triangle. In fact, except for the vibronic structures observed at high-energy positions, a very weak emission centered at 602 nm with lifetime 163 μs was also observed at 77 K glass (see Fig. 2). This structureless band is too low in energy to be one of the vibronic features from the π–π* excited state. Thus, this band is best assigned as a ^{3}MLCT transition on the basis of the absence of vibrational structure, although some incorporation of ^{3}π–π* character cannot be completely ruled out [31].

2.3. Host–guest interactions

Luminescent compounds with internal cavities have been demonstrated as having potential applications as chemosensory devices in recent years [27,37,38]. Many macrocyclic complexes have been studied for their molecular recognition capabilities toward small aromatic molecules, inorganic anions, or porphyrin molecules, based on their different cavity sizes and intermolecular forces such as hydrogen bonding, hydrophobic or electrostatic interactions [11,12]. Hupp et al. have elegantly demonstrated that different sized rhenium tricarbonyl based square complexes can effectively select different sized guest molecules by electrochemical transport experiments [39,40]. In fact, these square complexes are packed with infinite channels in their solid states [41–43]. Such properties make these macrocyclic molecules potential hosts for certain aromatic molecules in the solid state as well as in solution.

Whereas typical aromatic compounds encapsulated inside the metallocyclophane structures are not expected to result in significant changes in the luminescence properties, nitro-substituted aromatic compounds may be capable of serving as electron acceptors from the excited state and, thus, able to quench the luminescence. A series of nitro-substituted aromatic compounds (see Chart 3) have been used to test for quenching effects. In THF solution, the luminescence of both square **7** and its corner **14** are effectively quenched by these nitro-substituted aromatic compounds with quenching constants ranging from 4.94×10^8 to 9.12×10^9 M^{-1} s^{-1}.

In solid films, the luminescence spectral bands from both square **7** and corner **14** are blue shifted compared with their corresponding luminescence features in solution. This phenomenon is recognized as a luminescence rigidochromic effect [44,45]. In solution, the quenching constants are mainly determined by the electron-transfer rate from **7** or **14** to the quenchers and are, thus, dependent on the free energy change (ΔG°). For an oxidative electron-transfer reaction, ΔG° can be approximated according to $\Delta G^\circ = E_{ox} - E_{0-0} - E_{red}$, where E_{ox}, E_{0-0}, and E_{red} are oxidation potentials of **7** or **14**, the lowest triplet 0–0 excited state energy of **7** or **14**, and the reduction potentials of the quenchers, respectively. Given the higher E_{0-0} of corner **14** than E_{0-0} of square **7**, the quenching constants in THF solution for corner **14** are generally larger than the ones for square **7** [19].

However, in these solid films, more factors need to be considered to rationalize the luminescence quenching, namely, ΔG°, vapor pressure (VP) of the quenchers, and the binding constant (K_b). Fig. 3 compares the luminescence response of films of square **7** and corner **14** to the vapor of 2,3-dinitrotoluene (DNT) for 180 s. Clearly, only square **7** displays significant luminescence quench-

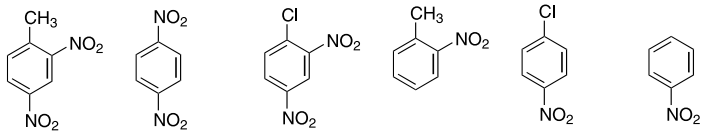

	DNT	**DNB**	**CDNB**	**NT**	**ClNB**	**NB**
rel. VP	6	1	3	7700	1000	10000
E_{red} (V)	-1.0	-0.7	-0.8	-1.28	-1.1	-1.15

Chart 3.

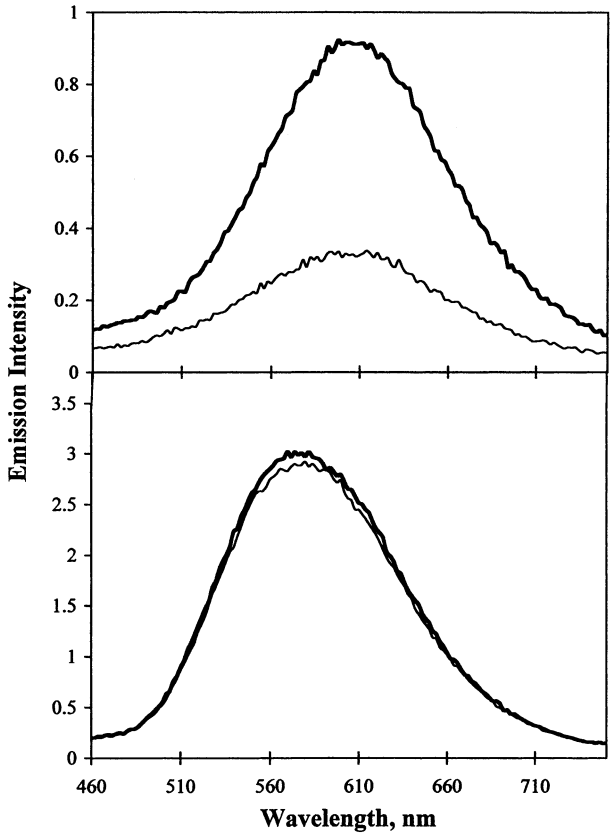

Fig. 3. Luminescence response of square **7** (top) and corner **14** (bottom) upon exposure to DNT vapor for 180 s. The thick and thin lines represent the luminescence before and after exposure to DNT vapor, respectively. Reprinted, with permission, from Ref. [19].

Table 2
The percent quenching of the luminescence of square **7** film after exposure to the vapor of different quenchers for 180 s

Analytes [a]	DNT	DNB	CNB	CDNB	NT	NB
% quenching	61	52	9.5	32	44	11

Data taken from Ref. [19].
[a] See Chart 3 for analytes' structures and abbreviations.

ing after exposure to the vapor of DNT in the solid film. The main factor that results in the significantly different quenching effect between the square **7** and corner **14** in the solid films is the difference in binding strength toward the quencher. The quenching effect appearing in the film of square **7** is apparently due to the porosity that exists in the film, which provides cavities for binding the quencher molecules [17,39,42]. Table 2 summarizes the quenching effects by different quenchers. In general, a higher VP from the quencher (that can bring higher numbers of binding molecules toward the square) and the incorporation of more nitro groups in the quenchers (providing a greater electronic interaction between the film and the quenchers) result in larger quenching effects [38].

3. Self-assembly organometallic squares with terpyridyl metal complexes as bridging ligands

3.1. Preparation of self-assembly octanuclear molecular squares linked by a metal-complex ligand

Squares **21**–**23** were prepared by reaction between $BrRe(CO)_5$ and the metal-complex bridging ligands in refluxing CH_3CN–THF mixture (see Scheme 4). Square **24** was prepared by reaction between $(dppf)Pd(H_2O)_2(OTf)_2$ and **19** in CH_3NO_2 solution (see Scheme 5). The corner complex **25** was prepared in low yield by removing the iron atoms from square **21** following a literature procedure (see Scheme 6) [46,47]. In each of the squares **21**–**23**, four possible diastereomers with respect to the relative positions of CO and Br^- may exist [18,41]. In Scheme 4, we do not intend to specify any isomer that is preferentially formed during the self-assembly process.

3.2. Photophysical properties

Electronic absorption and luminescence data recorded from the squares **21**–**24**, corner **25**, metal-complex bridging ligands **18**–**20**, and free ligand **17** (4′-(4‴-pyridyl)-2,2′:6′,2″-terpyridine) are summarized in Table 3. Fig. 4 shows the absorption spectra of squares **21**–**24**. All four squares display broad and intense visible absorptions in the region 400–600 nm, which are assigned to metal (Fe, Ru, or Os)-to-ligand (**17**) charge transfer (MLCT) bands [48]. Square **23** exhibits an additional weak band at 676 nm which is assigned to an Os-based ^{3}MLCT (Os-^{3}MLCT) band [48,49]. For each complex, the bands centered between 279 and 377 nm are assigned to ligand **17**-based π–π* bands and the Re-based MLCT band on consideration of the absorption spectra of ligand **17** and corner **25**. The formation of Re(I) based square complexes shifts the MLCT band to lower energy when compared with their metal-complex bridging ligands. Coordination of the free 4-pyridyl ring in the metal-complex ligand to the Re(I) center lowers the π* orbital localized on **17** and, thus, red shifts the corresponding MLCT band. Similar red-shifting behavior has also been observed when these metal-complex ligands are protonated or methylated in the 4-pyridyl positions [48].

For squares **21** and **22**, the MLCT band red shifts 599 and 412 cm^{-1} relative to **18** and **19**, respectively. The red shifting of the MLCT bands in square **23** is less prominent; the ^{1}MLCT band is 168 cm^{-1} red-shifted and the ^{3}MLCT band is red-shifted 177 cm^{-1}, compared with the corresponding MLCT bands in **20**. In the

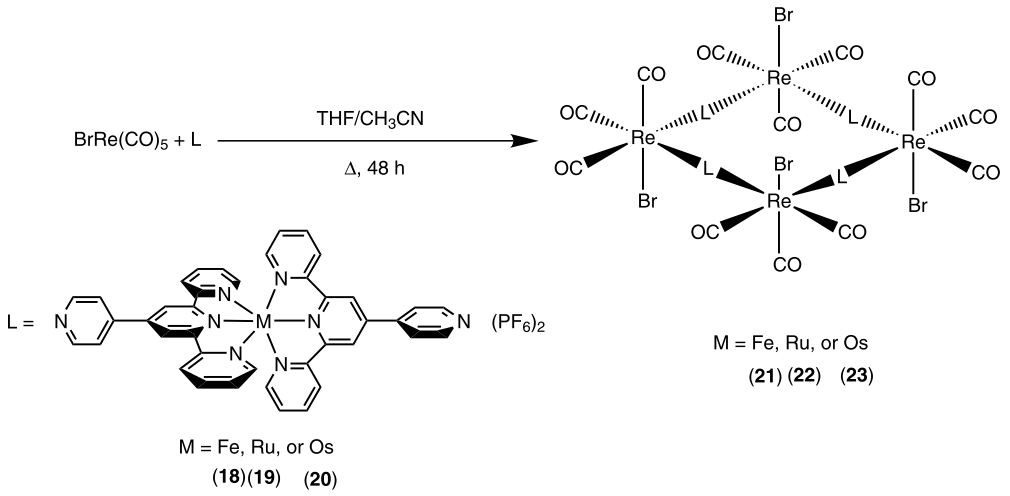

Scheme 4.

case of square **24**, the Ru(II)-to-**17** MLCT band does not shift in comparison to the MLCT band in **19**. The electron-donating dppf ligand certainly plays an important role here as it reduces the electron-accepting ability in Pd(II).

Squares **21**, **22** and **24** do not have any detectable solution luminescence at r.t. even though both the ligand **17** and the corner **25** emit in r.t. solution. The corner **25** exhibits luminescence at 538 nm in CH_3CN with a lifetime of 646 ns, which is typical of ^{3}MLCT emission. Ligand **17** emits at 359 nm in CH_2Cl_2 with a lifetime of 1.4 ns. The small Stokes shift and very short lifetime indicate that the emission originates from a singlet π–π* excited state. The lack of luminescence at r.t. from squares **21**, **22** and **24** is attributed to the existence of metal-centered (MC) states lying in close proximity to the MLCT states. The distortion from perfect octahedral structure, due to the C_{2v} symmetry in M(pyterpy)$_2$ (M = Fe, Ru), results in a relatively weak ligand field at the metal and, thus, the MC states are at low energy [50,51]. The MLCT excited states appear to be deactivated through these low-lying non-emissive MC states via an efficient nonradiative decay pathway. The low-lying MC states localized in ferrocenyl moieties in square **24** also provide an additional radiationless relaxation pathway for the deactivation of the MLCT excited states [52].

In contrast, square **23** exhibits r.t. luminescence in deoxygenated CH_3CN solution (see Fig. 5). The origin of the emission is assigned to a Os(II) based ^{3}MLCT transition. The stronger ligand field and lower oxidation potential of Os(II) compared with Ru(II) and Fe(II) results in an increased energy gap between the ^{3}MLCT and ^{3}MC states [53]. Therefore, it can be inferred that the ^{3}MC excited states are not so readily thermally populated in square **23**. The luminescence of square **23** exhibits a lower energy emission feature with a shorter lifetime and lower quantum yield compared with **20** (Table 3). This observation is in accordance with the energy gap law and is a consequence of the more efficient nonradiative decay in square **23** than **20** [54]. The quantum yield and position of emission of square **23** is also independent of the excitation wavelength and excitation of square **23** at 380 nm, where the Re(I) moiety is the sole chromophore, results in a luminescence band centered at 676 nm. The same luminescence position is also observed when square **23** is excited at 490 nm. The wavelength independent luminescence band implies that the energy transfer from higher energy states (Re-MLCT or π–π*) to the lowest Os-^{3}MLCT state is very efficient and close to unity.

Fig. 6 illustrates the spectral overlap between the absorption band of square **23** and the emission feature of corner **25**. The spectral overlap occurs from the red-edge of the singlet absorption band to the triplet absorption band. Thus, it can be concluded that the intramolecular energy transfer is most likely to be a triplet–triplet process. The complete quenching of the emission from the Re(I)-based donor in square **23** indicates that the energy transfer rate is much faster than 1×10^{10} s^{-1} [55,56]. According to MM2 molecular modeling, the Re(I)-to-Os(II) separation and the distance between the edges of the coordinating ligands are 10.9 and 1.5 Å, respectively. Given that there is a such short distance of separation between the Re(I) donor and Os(II) acceptor as well as the large triplet character involved, it can be concluded that the energy transfer occurs likely via a Dexter-type electron exchange process [57], although the participation of a Förster-type dipole–dipole mechanism can not be completely ruled out [58]. A qualitative energy level diagram of square **3** is summarized in Scheme 7, depicting the energy levels and processes of the Re and Os based moieties.

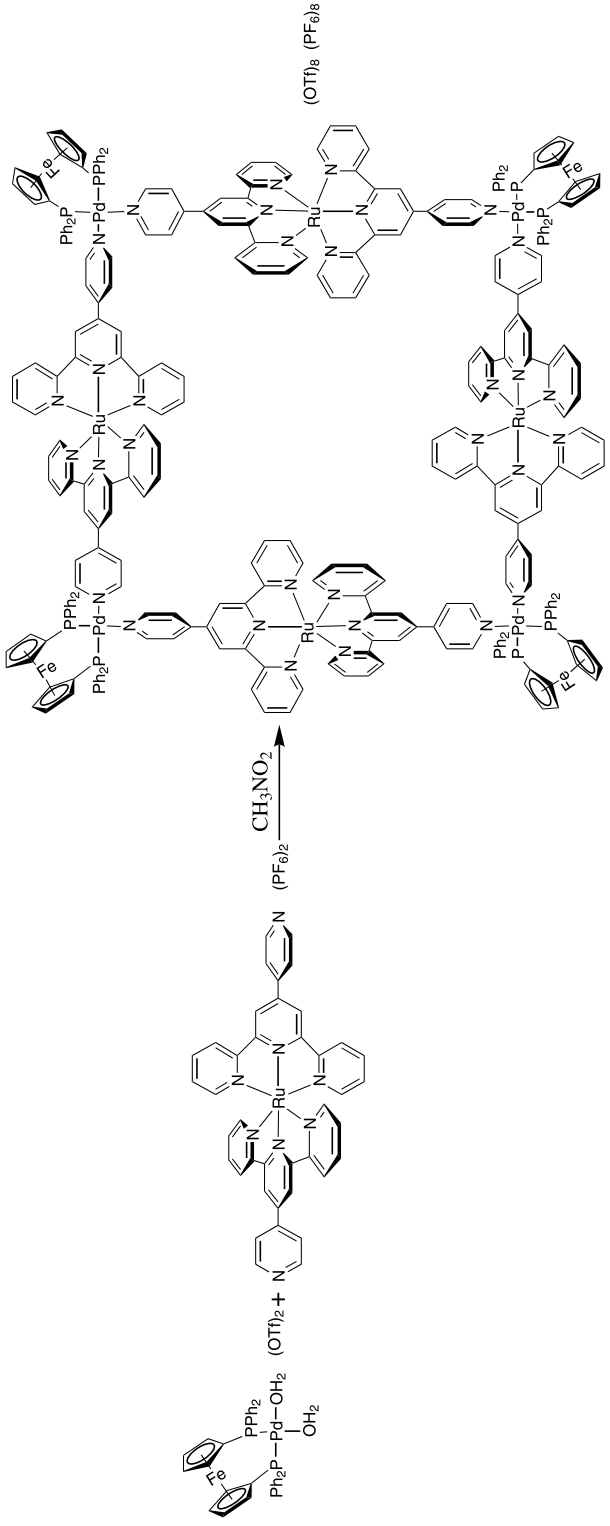

Scheme 5.

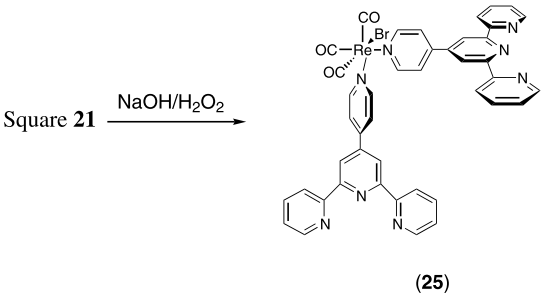

Scheme 6.

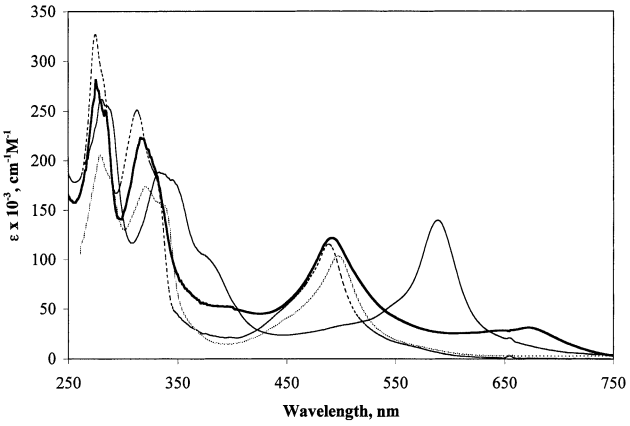

Fig. 4. Electronic absorption spectra of squares **21**–**24** in DMSO (squares **21** (solid line) and **22** (thin dash line)) or CH_3CN (squares **23** (thick solid line) and **24** (dashed line)) at 293 K. Reprinted, with permission, from Ref. [21].

3.3. Host–guest interactions

The highly positive charges and luminescent behavior of square **23** have prompted us to study its potential use as a host for inorganic anionic species [17,26]. We have tested several inorganic polyatomic anions such as BF_4^-, CH_3COO^-, PF_6^-, and OTf^- with the expectation of observing changes in luminescence intensities that arise from host–guest interactions. Unfortunately, in this particular square molecule, we have found that the emission results are irreproducible and noted that decomposition of square **23** was usually observed when excess anions were added into the solution containing this complex. The large internal cavity of square **23**, which minimizes the electrostatic and/or any hydrophobic interactions between square **23** and guest anions, as well as the difference in stability provided by counter ions may account for the square decomposition and the irreproducibility of the results.

4. Self-assembly organometallic molecular cages comprising of 11 components

Three-dimensional structures usually provide larger interior voids for guest encapsulation over other two-dimensional structures and, therefore, they are better synthetic targets from the perspective of developing supramolecular catalysts where the relatively large catalytic environments are required to accommodate the reactants [16,59]. To date, most of the one step self-assembly transition-metal-containing supramolecular species reported in the literature have been synthesized from the same metal components and bridging ligands [9–13]. The one-pot formation of three dimensional cages incorporating different metal components or more than two different types of bridging ligands is much rarer due to the strong enthalpy effect [60–65]. As an

Table 3
Electronic absorption and emission spectra of molecular squares and their metal-complex bridging ligands at 293 K

Compounds	Absorption spectra	Emission		
	λ_{max}, nm ($\varepsilon \times 10^{-3}$, M^{-1} cm^{-1})	λ_{max}, nm	τ, ns	Φ_{em} [a]
21 [b]	281 (279), 333 (200), 345 (192), 377 (107), 588 (147)	[c]		
22 [b]	279 (278), 320 (175), 332 (159), 498 (133)	[c]		
23 [d,e]	238 (196), 275 (281), 318 (222), 402 (49.4), 490 (122), 676 (30.9)	748	42	4.2×10^{-4}
24 [d]	236 (242), 275 (327), 313 (251), 331 (181), 488 (115)	[c]		
25 [d,f]	244 (80.9), 274 (62.8), 317 (33.0), 379 (sh, 6.55)	530	646	1.8×10^{-3}
18 [d]	245 (62.9), 276 (93.8), 283 (102), 324 (60.8), 334 (55.5), 374 (9.2), 568 (34.2)	[c]		
19 [d]	240 (58.9), 276 (95.0), 313 (61.1), 333 (48.5), 488 (36.3)	[c]		
20 [d]	239 (48.4), 276 (68.3), 317 (56.3), 394 (11.1), 486 (27.3), 668 (7.1)	740	67	6.7×10^{-4}
17 [g]	244 (38.5), 279 (26.2), 315 (8.8)	359	1.4	7.0×10^{-2}

Data taken from Refs. [16,17].
[a] Quantum yield is calculated relative to $Os(bpy)_3(PF_6)_2$ ($\Phi_{em} = 0.005$ in CH_3CN).
[b] DMSO solution.
[c] No luminescence detected.
[d] CH_3CN solution.
[e] $\lambda_{ex} = 490$ nm.
[f] $\lambda_{ex} = 380$ nm. Quantum yield is calculated relative to [(bpy)Re(CO)$_3$(4-Etpy)](PF$_6$) ($\Phi_{em} = 0.027$ in CH_3CN).
[g] CH_2Cl_2 solution, $\lambda_{ex} = 320$ nm. Quantum yield is calculated relative to 9,10-diphenylanthracene ($\Phi_{em} = 0.95$ in EtOH).

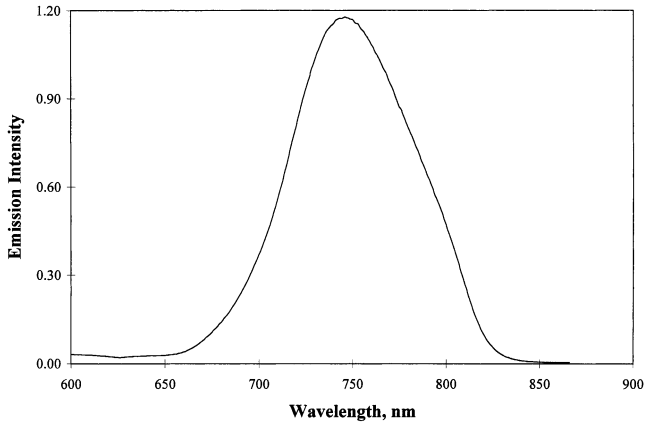

Fig. 5. Emission spectrum of square **23** in deoxygenated CH_3CN solution at 293 K. Reprinted, with permission, from Ref. [21].

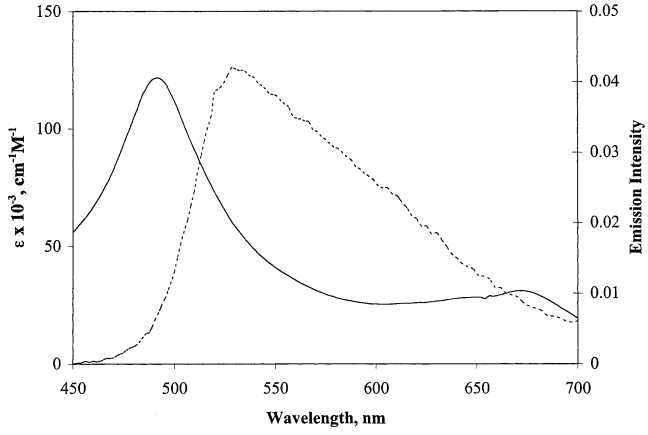

Fig. 6. Spectral overlap between absorption spectrum of square **23** (solid line) and emission spectrum of corner **25** (dashed line) in deoxygenated CH_3CN solution.

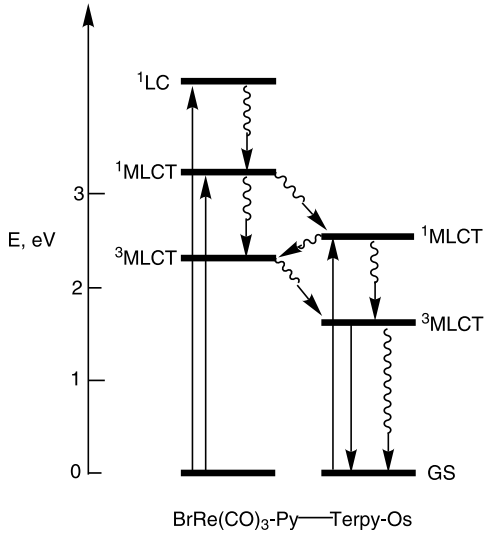

Scheme 7.

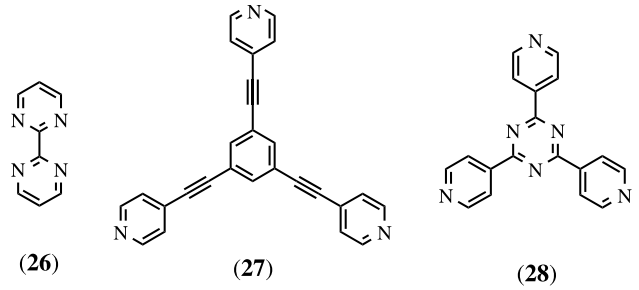

Chart 4.

extension of our previous work, we set out to design and synthesize self-assembly cage-type molecules that comprise two different types of ligands, which require more precise binding angles between the metal components and the bridging ligands in order to avoid the formation of undesired oligomeric species.

4.1. Preparation of self-assembly molecular cages

Two synthetic routes to these cage molecules have been investigated (see Chart 4 and Scheme 8). The first involved synthesis of the ligand **26** bridged dinuclear Re(I) complex **29** and subsequent replacement of the bromo ligand by triflate (OTf) in acetone to isolate complex **30** [66,67]. Subsequent reflux of **29** and the corresponding tridentate ligands, **27** or **28** in THF for 3 days afforded reddish products with general formula $\{[fac\text{-}Re(CO)_3]_2(\mu\text{-BPM})\}_3(\mu\text{-L})_2(OTf)_6$ (**31**, L = **27**; **32**, L = **28**) [68].

Alternatively, the cages **31** and **32** can be prepared in a simpler one-step process (Scheme 8). The synthesis was initiated by refluxing $(OTf)Re(CO)_5$, (**26**), and L (**27** or **28**) in a 6:3:2 ratio in THF for 1 week and, subsequently, cages **31** and **32** were isolated in 47 and 41% yield, respectively. The ligand **26** bridged dimer, $[(CO)_3ReOTf]_2(\mu\text{-}\mathbf{26})$, would be expected to form first in the solution considering the extra stabilization through this bridging ligand's chelation effect. Indeed, the formation of one precursor, which is more thermodynamically stable than the other possible intermediates, is important for a self-assembly process that comprises more than one bridging ligand. Subsequently, the thermodynamically driven self-assembly process between $[(CO)_3ReOTf]_2(\mu\text{-}\mathbf{26})$ and the corresponding **27** and **28** ligands afforded the final cage products.

4.2. Photophysical properties

The absorption spectra of **31** and **32** in CH_3CN feature intense bands in the near-UV region and a low-energy band at 470 nm, tailing past 600 nm (see Fig. 7). This low energy band is assigned to the Re(dπ) to ligand **26** (π*) charge-transfer transition (MLCT). Both **31** and **32** are non-emissive in r.t. CH_3CN solution. Several ligand **26**-bridged Re(I) tricarbonyl complexes have

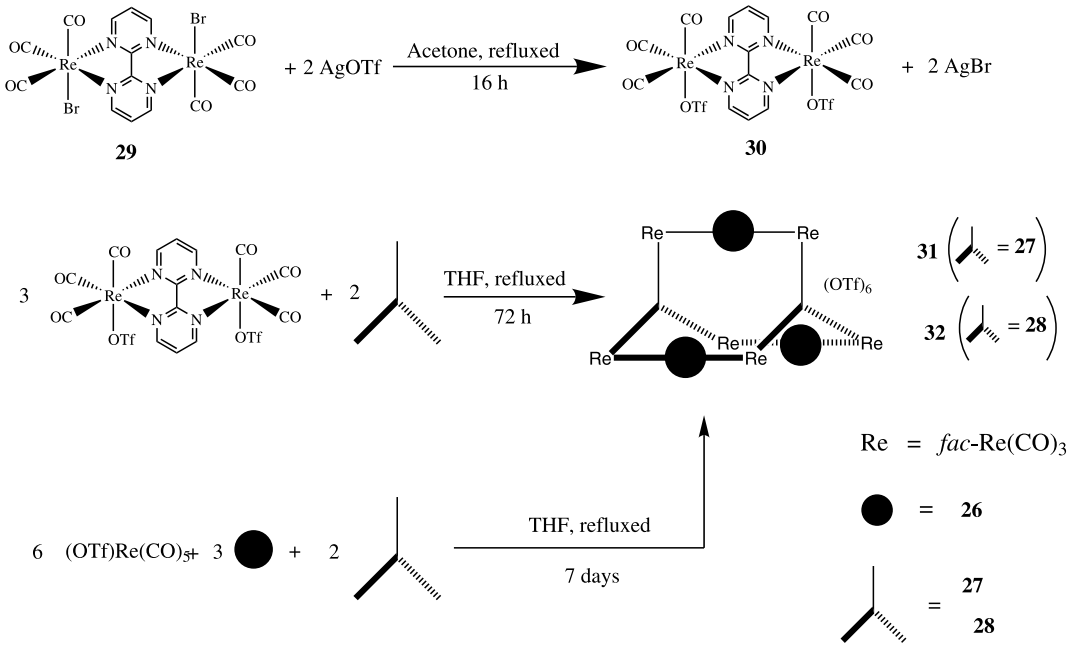

Scheme 8.

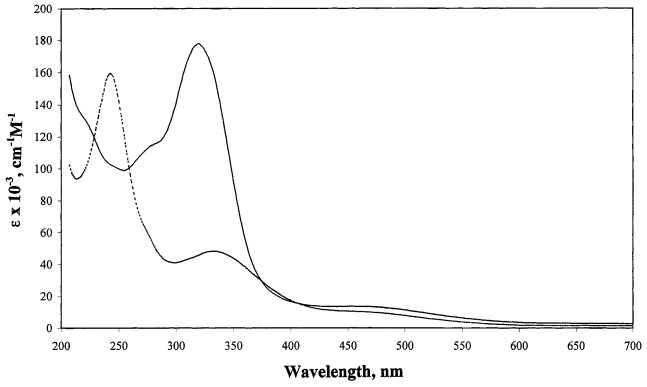

Fig. 7. Electronic absorption spectra of cages **31** (solid line) and **32** (dashed line) in CH_3CN at r.t.. Reprinted, with permission, from Ref. [22].

been reported that exhibit a lack of emission [67,69]. These observations have been attributed to the energy gap law effect [30], resulting in the low-energy ^{3}MLCT excited state undergoing very efficient nonradiative decay. However, it is also possible that an emission band is present but is too red-shifted to detect on our instrumentation.

4.3. Host–guest interactions

According to MM2 molecular modeling results, the interplanar distances between the two tridentate ligands in **31** and **32** are 3.5 and 4.2 Å, respectively. These interplanar distances are comparable to the recently reported rectangular structures [70,71] and the molecules are considered to have very effective π–π stacking

Table 4
The association constants (K_a, M^{-1}) of molecular cages **31** and **32** with different guests

Guests	31	32
o-Dimethoxybenzene	0.81×10^2	0.99×10^2
m-Dimethoxybenzene	5.9×10^2	6.1×10^2
p-Dimethoxybenzene	4.5×10^2	4.2×10^2
1,3,5-Trimethoxybenzene	8.9×10^2	9.1×10^2
2-Naphthalenesulfonic acid, sodium salt	11.2×10^2	11.6×10^2
1,5-Naphthalenedisulfonic acid, disodium salt	26.4×10^2	20.7×10^2
2,6-Naphthalenedisulfonic acid, disodium salt	15.6×10^2	13.8×10^2
Sodium tetraphenylborate	0.75×10^2	0.60×10^2
p-Dimethoxycyclohexane	$< 0.01 \times 10^2$	$< 0.01 \times 10^2$

Data taken from Ref. [18]. Binding was monitored by following the phenyl proton of ligand **27** for cage **31** and β proton of ligand **28** for cage **32**. The spectra were recorded at 300 MHz in DMSO-d_6 solution at 298 K.

that contributes to the highly thermodynamically stable structures [60,62]. The nearly co-planar arrangement between the two tridentate ligands and the overall six positive charges in **31** and **32** render them as promising hosts for electron-rich planar aromatic compounds. Table 4 summarizes the association constants (K_a) of **31** and **32** with different aromatic compounds. Not surprising, there is virtually no association between *p*-dimethoxycyclohexane and either **31** or **32** and only a very small association between spherical sodium tetraphenylborate and **31** or **32**. On the other hand, both **31** and **32** showed relatively strong association toward planar aromatic compounds. There are no clear binding

differences between **31** and **32**. The shape selectivity, however, deserves more attention and is being further investigated. A significant difference in K_a values was observed for the isomers of dimethoxybenzene, where *m*- and *p*-dimethoxybenzene ≫ *o*-dimethoxybenzene. A similar trend of shape selectivity has also been observed for Pd and Pt based square complexes [70].

5. Photoswitchable trinuclear *fac*-(diimine)Re(I)(CO)$_3$ complexes linked by a stilbene-like bridging ligand

The light-driven *cis*–*trans* isomerization processes of stilbenes and compounds containing stilbene units have received active investigation both on fundamental studies and practical applications [71–73]. The *cis*- or *trans*-stilbenes and their analogues are good triplet energy acceptors for exploring photosensitization and energy transfer processes [32,74–80]. We have synthesized a series of trinuclear metal complexes containing *fac*-(diimine)Re(I)(CO)$_3$ chromophores bridged by a stilbene-like tridentate ligand [23]. The results show that following excitation into the Re (dπ) → diimine (π*) MLCT manifold, efficient triplet–triplet energy transfer from the ^{3}MLCT state to the bridging ligand occurs and this results in *trans*–*cis* isomerization of the bridging ligand.

5.1. Synthesis

The structures of the bridging ligands and complexes reported in this section are shown in Chart 5. Complexes [(NN)Re(CO)$_3$]$_3$(μ-**33**)(PF$_6$)$_3$ and [(NN)Re(CO)$_3$]$_3$(μ-**27**)(PF$_6$)$_3$, where NN = bpy, 4,4′-dimethyl-bpy (Me$_2$-bpy) or 4-nitro-bpy (NO$_2$-bpy), and **33** = 1,3,5-tris(2-ethenyl-4-pyridyl)benzene, were synthesized by refluxing a 3:1 molar ratio of (NN)Re(CO)$_3$(CH$_3$CN)(PF$_6$) and **33** or **27** in THF solution and then standard workup procedures [81,82].

5.2. Photophysical properties and photoinduced isomerization

Photophysical parameters obtained from compounds **34**–**38** are summarized in Table 5. The absorption spectra of all these compounds feature a series of ligand localized π → π* and metal (dπ) to ligand (π*) charge transfer (MLCT) bands. Unlike most metal complexes containing the *fac*-(diimine)Re(I)(CO)$_3$ unit which are typically highly luminescent in solution [3,28,82], compounds **34** and **35** show only weak luminescence ($\Phi_{em} < 0.0015$) in r.t. CH$_3$CN solution. The quenching appears to occur via intramolecular sensitization of the π → π* transition localized on the olefin link of the bridging ligand accompanied by a *trans*–*cis* isomerization process (Eq (1)).

$$[(NN)Re^{I}(CO)_3]_3(\mu\text{-}trans\text{-}\mathbf{33}) \xrightarrow{h\upsilon} [^3(NN^{\bullet-})Re^{II}(CO)_3]_3{}^*(\mu\text{-}trans\text{-}\mathbf{33}) \underset{k_{ENT}}{\overset{k_{ENT}}{\rightleftharpoons}}$$
$$[(NN)Re^{I}(CO)_3]_3{}^3(\mu\text{-}trans\text{-}\mathbf{33})^* \xrightarrow[\text{isomerization}]{trans\text{-}cis} [(NN)Re^{I}(CO)_3]_3(\mu\text{-}cis\text{-}\mathbf{33}) \quad (1)$$

Table 5
Photophysical properties of trinuclear compounds **34**–**38**

Compounds	Absorption spectra	Emission						
	λ_{max}, nm (10^{-3} ε, M^{-1} cm^{-1})	λ_{max}, nm	10^2 Φ_{em} [a]	τ, ns	k_r, s^{-1}	k_{nr}, s^{-1}	k_{ENT}, s^{-1} [b]	Φ_{eff} [c]
34	341 (85), 320 (88), 280 (48), 239 (49)	574	0.14	15.1	9.3×10^4	3.1×10^6	6.3×10^7	0.94
35	341 (94), 318 (86), 280 (50), 240 (55)	562	0.099	10.2	9.9×10^4	1.9×10^6	9.8×10^7	0.98
36	402 (sh, 21), 336 (90), 285 (sh, 57), 238 (60)	[d]						
37	342 (sh, 47), 319 (88), 301 (94), 283 (84), 251 (66)	576	3.03	246	1.2×10^5	3.9×10^6		
38	326 (sh, 75), 316 (95), 304 (94), 288 (79), 251 (71)	566	6.11	507	1.2×10^5	1.9×10^6		

Data taken from Ref. [19]. The excitation wavelengths are 380 nm.
[a] The emission quantum yields were determined using (bpy)Re(CO)$_3$(4-Etpy)(PF$_6$) ($\Phi_{em}^{CH_3CN} = 0.027$) and perylene ($\Phi_{em}^{EtOH} = 0.89$) as references.
[b] Triplet–triplet energy transfer rate constant.
[c] Quantum yield for generating ^{3}ππ* excited state localized on ligand **33**.
[d] No detectable emission.

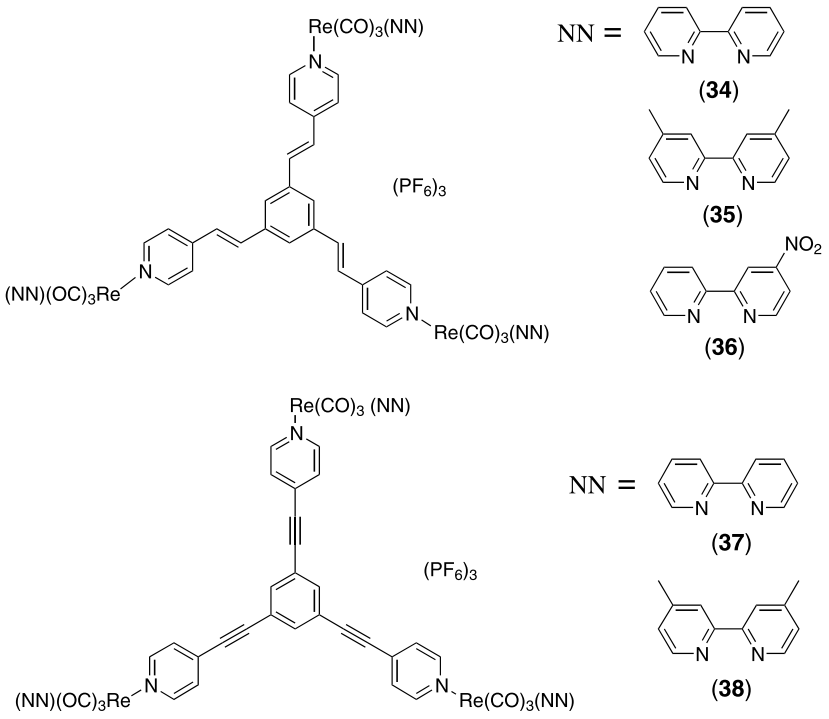

Chart 5.

Eq. (1) is supported by steady-state photolysis experiments. Fig. 8 shows the difference absorption spectrum of compound **34** in CH_3CN solution as a function of photolysis time. Photolysis into the MLCT band at 366 nm bleaches the ππ* absorption of the bridging ligand at ca. 280–370 nm and induces small increases at ca. 200–270 nm. A similar bleaching effect at ca. 280–330 nm was also observed for free ligand **33** photolyzed at 313 nm. Furthermore, changes observed in the emission are very substantial and the emission quantum yield is 18 times greater for **34** (see inset in Fig. 8) and 21 times stronger for **35** after 7 h photolysis at 366 nm compared with the original spectra. The UV–vis spectral changes and large increase in the luminescence intensity for **34** and **35** are consistent with the *trans–cis* isomerization of the bridging ligand, **33**, and highly efficient energy transfer [32,76]. The energy transfer from the ^{3}MLCT state to the higher energy triplet excited state localized on the *cis*-configuration bridging ligand is blocked or, at least, becomes more unfavorable than the direct deactivation from ^{3}MLCT excited state to the ground state.

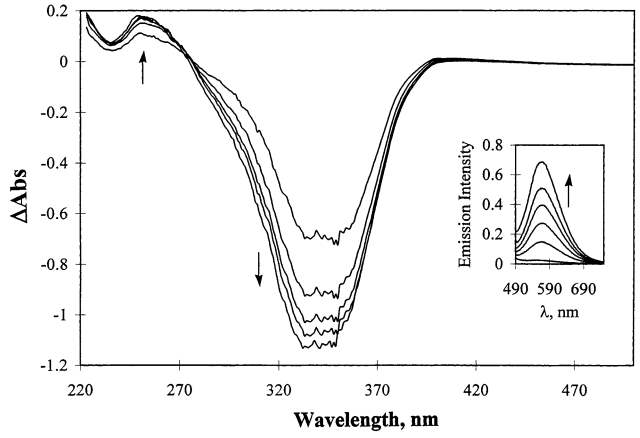

Fig. 8. UV–vis difference absorption spectra ($\Delta_{Abs} = A_t - A_{t=0}$) of compound **34** in CH_3CN at 293 K as a function of photolysis time (λ_{ex} = 366 nm; 0, 1, 2, 3, 4, 6 h). The inset shows the emission spectra before and after photolysis. Reprinted, with permission, from Ref. [20].

On the other hand, there is no emission detected from **36** even after prolonged irradiation at 366 nm for 48 h. The lack of emission from **36** is attributed to the energy gap law; that is, the lower energy ^{3}MLCT excited state results in a better vibrational overlap between the ground and excited states and the nonradiative decay increases as the vibrational overlap increases [30]. The low energy ^{3}MLCT excited state in **36** also makes the energy transfer process energetically unfavorable.

Assuming that the MLCT intersystem crossing efficiency is unity, and radiative (k_r) and nonradiative (k_{nr}) decay to the ground state and energy transfer (k_{ENT}) to **33** are the only deactivation processes for the ^{3}MLCT excited state, and that the decay from the ^{3}ππ* excited state localized on ligand **33** is much faster than energy transfer, then Φ_{em} and τ for [(NN)Re(CO)$_3$]$_3$(μ-**33**)(PF$_6$)$_3$ can be expressed as: $\Phi_{em} = k_r/(k_r + k_{nr} + k_{ENT})$ and $\tau = (k_r + k_{nr} + k_{ENT})^{-1}$. Calculated photophysical parameters are shown in Table 5. As expected, all the k_r values are very similar, ca. 1×10^5 s^{-1}, for the series of *fac*-(diimine)Re(I)(CO)$_3$L complexes and in agreement with related Re(I) chromophores [31]. The

energy transfer rate constant, k_{ENT}, and the efficiency for generating the $^3\pi\pi^*$ excited state localized on ligand **33**, Φ_{ENT}, at 293 K can be determined based on: $k_{ENT} = \tau^{-1} - \tau_{model}^{-1}$ and $\Phi_{ENT} = k_{ENT}/(k_r + k_{nr} + k_{ENT})$ with **37** and **38** as model compounds and their values are also listed in Table 5.

It is not surprising that both k_{ENT} and Φ_{ENT} values for **35** are larger than the corresponding values for **34**. The higher ^{3}MLCT excited energy in **35** results in a larger energy gap between the triplet donor and acceptor and, thus, a larger driving force that enhances the efficiency of energy transfer process. In summary, we have demonstrated that the emission from *trans*-**33** bridged trinuclear Re(I) complexes can be 'turned on' by highly efficient photoinduced energy transfer from a ^{3}MLCT excited state to a bridged ligand localized $^3\pi$–π^* excited state followed by ligand isomerization.

6. Complexes exhibiting luminescent anion receptor behavior via hydrogen bonding

The design and synthesis of efficient artificial receptors for selective binding of biologically or environmentally important anionic species represent an emerging field with many applications. A variety of synthetic receptors have been designed and studied for their binding strength and selectivity toward different anions. A number of review articles have appeared which have covered many different aspects of anion receptor systems [83–89]. Despite many of these receptors showing excellent selectivity, they usually have very elaborate structures that typically require multiple synthetic steps with relatively low overall yields which make it impractical to prepare them on a large scale.

Nature provides many examples of proteins utilizing hydrogen bonding for binding substrates [90]. The incorporation of luminescent chromophores into the receptor which are sensitive to interactions between the receptor and analytes has gained considerable attention due to their high sensitivity and detection limit [27]. The appeal of sensors containing luminescence chromophores stems from the high sensitivity of luminescence detection compared with other spectroscopic methods. The binding of anionic species to the recognition sites leads to changes in certain properties of the receptors (such as luminescence, lifetime, etc.) which then serve as an indicator of guest association. Although there have been several literature reports concerning luminescence-based anion detection [27,91,92], the highly sensitive luminescence-based fluoride and cyanide sensory systems are much rarer [91,92]. During the course of our investigation toward the potential luminescence metal-complex receptor, we have found a structurally very

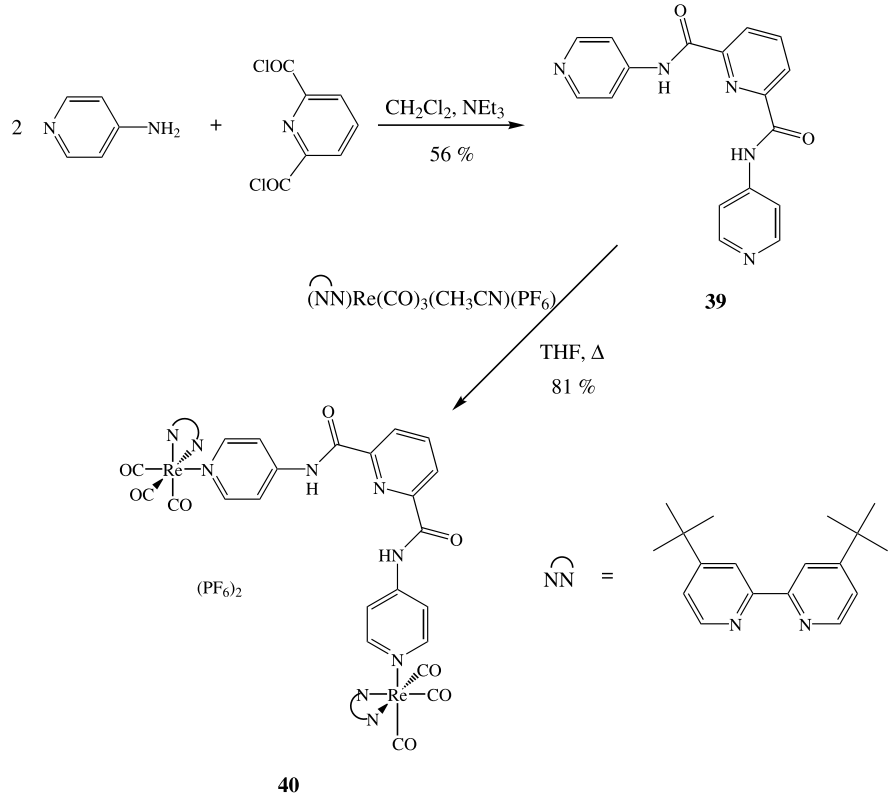

Scheme 9.

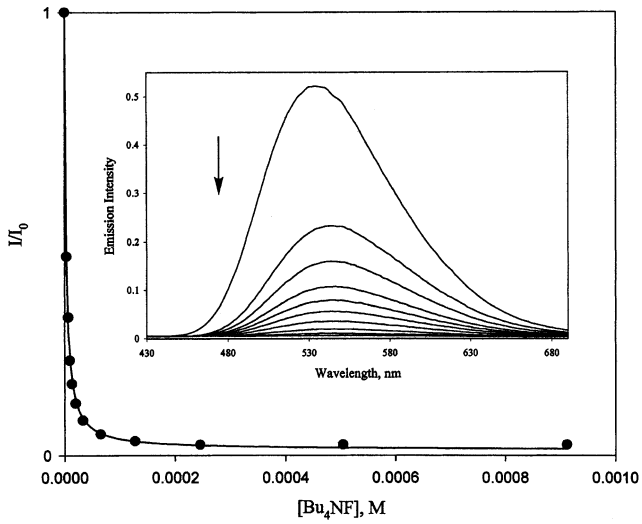

Fig. 9. Titration curve of the addition of F^- anion (as tetrabutylammonium salt). The inset shows the change of the emission intensity of complex **40** in CH_2Cl_2 solution upon addition of F^- anion. Excitation wavelength is 360 nm. Reprinted, with permission, from Ref. [24].

simple yet highly sensitive and selective luminescent anion receptor which shows high affinities for halides, cyanide and acetate anions with binding constants as high as 10^4–10^5 M^{-1} and a detection limit as low as 10^{-8} M in CH_2Cl_2 solution.

6.1. Synthesis and physical properties

The synthesis of bridging ligand **39** and complex **40** is shown in Scheme 9. The bridging ligand **39** was prepared in 56% yield from two equivalent of 4-aminopyridine and 2,6-pyridinedicarbonyl dichloride. Subsequent reaction of **39** and two equivalents of $(CH_3CN)(t\,Bu_2bpy)Re(CO)_3(PF_6)$ in refluxing THF, followed by recrystallization from CH_2Cl_2–pentane, afforded a bright yellow crystalline solid **40** in 81% yield.

Table 6
Binding constants, K_b, of different anions toward dinuclear complex **40** determined by luminescence titration in CH_2Cl_2 at 298 K

Anions	K_b, M^{-1}
CN^-	8.80×10^5
F^-	3.82×10^5
Cl^-	3.99×10^4
Br^-	3.90×10^4
I^-	1.49×10^5
OAc^-	3.41×10^4
$H_2PO_4^-$	1.47×10^2
NO_3^-	63.4
ClO_4^-	8.4

Data taken from Ref. [20].

The N–H protons of complex **40** exhibit a chemical shift of 10.59 ppm in $CDCl_3$. The very downfield chemical shift indicates the presence of strong intramolecular hydrogen bonding between the N–H protons and nitrogen in the central pyridine. This results in ligand **39** having an approximate right angle geometry [93–95] and the converged structure of complex **40** renders it as an effective anion receptor through hydrogen bonding interactions [96]. In deoxygenated CH_2Cl_2 solution, complex **40** exhibited intense absorption bands in the near UV and visible spectral region ($\lambda_{max} = 254$, 281, and 380 nm, $\varepsilon_{max} = 63\,600$, 61 500, and 7700 M^{-1} cm^{-1}, respectively) and a very strong luminescence at 536 nm with quantum yield of 0.37 and lifetime of 0.48 μs.

6.2. Anion sensing studies

Addition of different halides or inorganic polyatomic anions (as tetrabutylammonium salts) into a 1×10^{-5} M solution of complex **40** was observed to cause different degrees of quenching of the luminescence intensities. The N–H protons in ^{1}H-NMR spectra all showed significant downfield shifts (> 1.5 ppm), indicating the strong hydrogen bonding formation between the amide protons of complex **40** and the anions. Fig. 9 shows a typical titration curve for the luminescence intensity upon addition of F^- to a CH_2Cl_2 solution of **40**. The curve was determined to fit well to a 1:1 binding isotherm [97]. Concomitant with this quenching, the luminescence wavelength slightly red-shifted from 536 to 546 nm.

Table 6 summarizes the binding constants measured for complex **40** toward different anions. Clearly, this molecule shows strong binding affinity toward halides, cyanide, or acetate anions, only moderate binding affinity toward dihydrogen phosphate and very weak binding affinity to nitrate or perchlorate anions. The overall order determined for binding affinity is: $CN^- > F^- > I^- > Cl^- \sim Br^- \sim OAc^- \gg H_2PO_4^- > NO_3^- > ClO_4^-$. This finding is significant as it is not common for charged receptors to exhibit such outstanding selectivity for anion species [98]. In fact, the combination of interactions involving electrostatic force, hydrogen bonding strength, and steric effects all apparently influence the binding affinities toward anions in complex **40**. Importantly, the sensitivity of complex **40** is so high that the emission intensity can be effectively quenched by as much as 10% even in the presence of only 10^{-8} M cyanide or fluoride anions.

The origin of the emission quenching upon addition of anions is not certain at this stage. The red shift of the emission band, however, indicates that the emission quenching is associated with a change in the energy of the excited state and, thus, an enhancement of non-radiative decay. In summary, complex **40** represents a

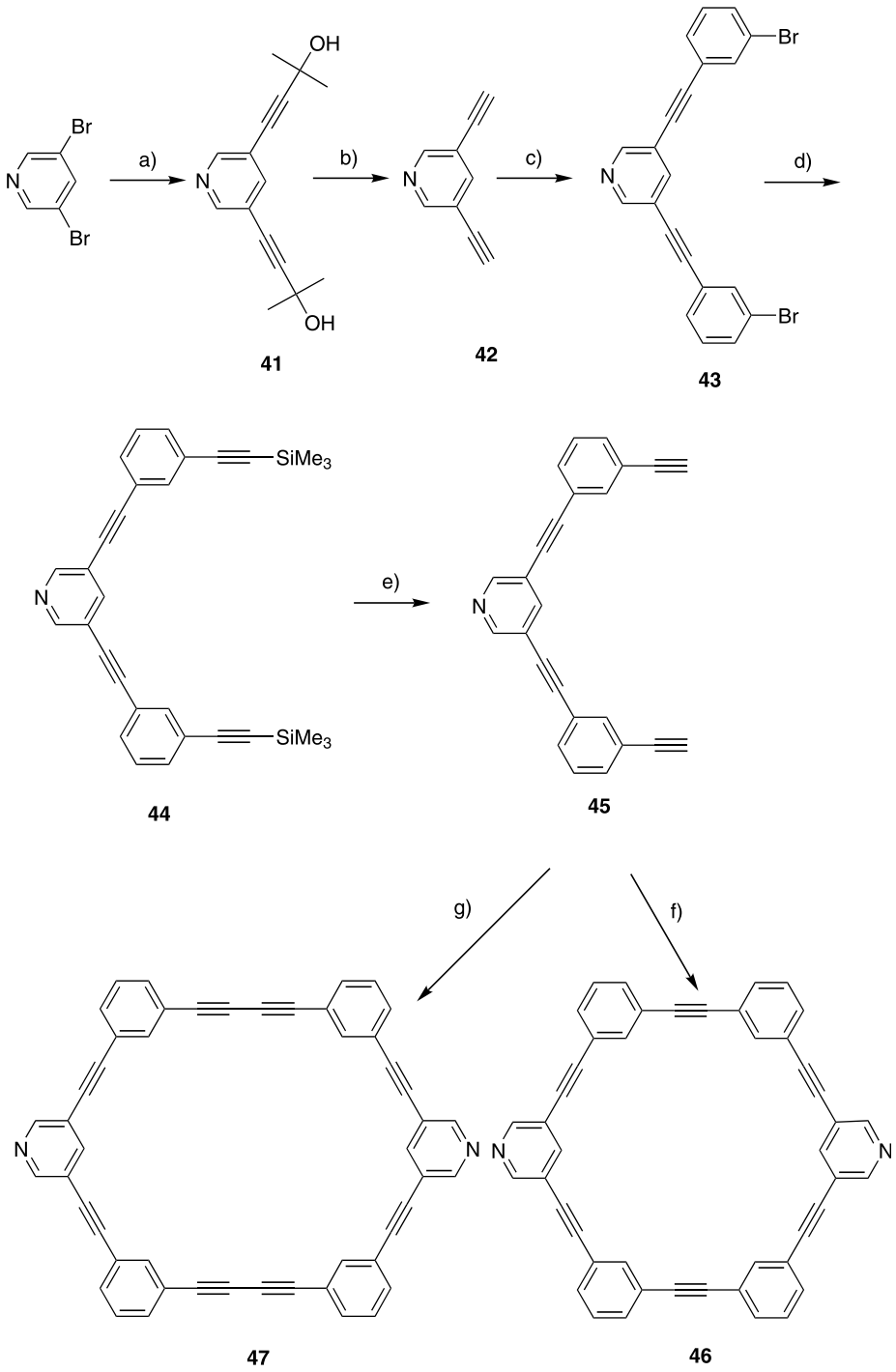

Scheme 10. (a) $PdCl_2(PPh_3)_2$, CuI, NEt_3/THF (1:1), 2-methyl-3-butyn-2-ol, 75 °C, 12 h, 91%; (b) KOH, benzene, refluxed, 5 h, 82%; (c) 1-bromo-3-iodobenzene, $PdCl_2(PPh_3)_2$, CuI, NEt_3/THF (1:1), 35 °C, 20 h, 76%; (d) $PdCl_2(PPh_3)_2$, CuI, *i*-Pr_2NH, trimethylsilylacetylene, 70 °C, 48 h, 59%; (e) KF, MeOH, room temperature, 24 h, 99%; (f) **43**, $PdCl_2(PPh_3)_2$, CuI, *i*-Pr_2NH, 70 °C, 16 h, 54%; (g) CuCl, pyridine, O_2, room temperature, 30 h, 32%.

simple and easy to prepare luminescent anion sensory system. The strong binding affinity and high selectivity of complex **40** for certain anions also may make it a promising candidate for many other different applications besides sensors, such as homogeneous catalysis [99–101] and membrane transport [102,103].

7. Dinuclear metal complexes bridged by macrocyclic phenylacetylenic ligands

Macrocyclic phenylacetylenes with defined shapes and geometries have drawn a great deal of attention in the last few years [104–106]. Several macrocyclic

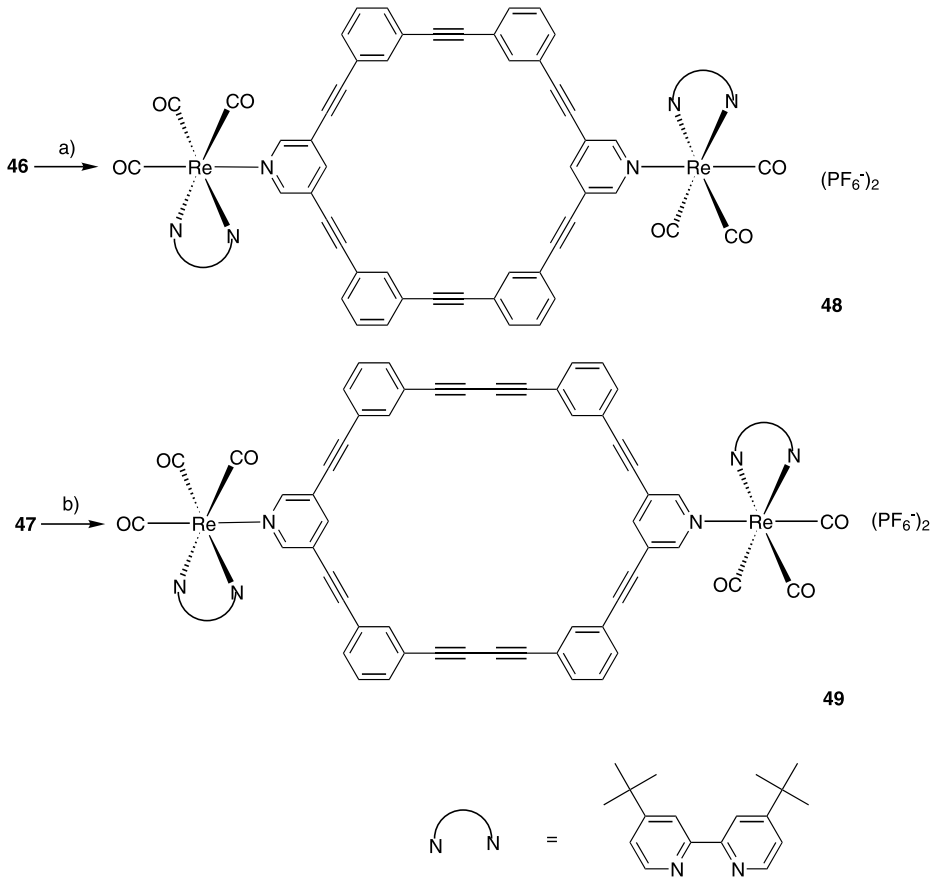

Scheme 11. (a) $(CH_3CN)Re(CO)_3$(4,4′-*tert*-Bu_2bpy)(PF_6), THF, 60 °C, 18 h, 62%. (b) $(CH_3CN)Re(CO)_3$(4,4′-*tert*-Bu_2bpy)(PF_6), THF, 60 °C, 3 days, 26%.

phenylacetylenes have been shown to have especially interesting properties, such as self-association in solution [104,105], the existence of liquid crystalline phases [107], formation of hydrogen-bonding solids with large internal voids [108], and the capability to bind small guest molecules [108–111]. These different properties can be easily modified by varying the size and shape of the molecules as well as the electronic and steric character of the substituents on the macrocyclic framework. Very recently, we have utilized a macrocyclic phenylacetylenic unit to link transition-metal chromophores [25]. Some interesting aspects are summarized below.

7.1. Synthesis

Stepwise synthetic procedures for the macrocyclic ligands **46** and **47** are illustrated in Scheme 10. Precursor **41** was readily synthesized from 3,5-dibromopyridine and 2-methyl-3-butyn-2-ol by a Sonogashira–Hagihara cross coupling reaction catalyzed by $Pd(PPh_3)_2Cl_2$ and CuI [112,113]. Subsequent deprotection of **41**, leading to

Table 7
Photophysical data of macrocyclic ligands (**46** and **47**) and associated dinuclear complexes (**48** and **49**) in deoxygenated CH_2Cl_2

Compounds	Absorption spectra	Emission		
	λ_{max}, nm ($\varepsilon \times 10^{-3}$, M^{-1} cm^{-1})	λ_{max}, nm	τ, ns	Φ_{em} [a]
46 [b]	252 (54), 262 (60), 288 (41.2), 303 (32.9)	337	1.2	0.19
47 [b]	240 (43.2), 249 (46.1), 275 (sh, 35.0), 287 (42.2), 300 (33.4)	336	1.1	0.15
48	251 (116), 272 (121), 281 (120), 305 (102), 316 (sh, 81.3), 344 (sh, 23.1), 380 (sh, 9.31)	542	1060	0.026
49	251 (156), 261 (154), 283 (sh, 111), 303 (94.9), 316 (sh, 80.6), 346 (sh, 24.9), 380 (sh, 9.31)	540	1010	0.026

Data taken from Ref. [21]. $\lambda_{ex} = 350$ nm.

[a] Quantum yield is calculated relative to $[(bpy)Re(CO)_3(4\text{-Etpy})](PF_6)$ ($\Phi_{em} = 0.027$ in CH_3CN) for dimers **48** and **49** or calculated relative to aniline ($\Phi_{em} = 0.10$ in EtOH) for ligands **46** and **47**.

[b] $\lambda_{ex} = 310$ nm.

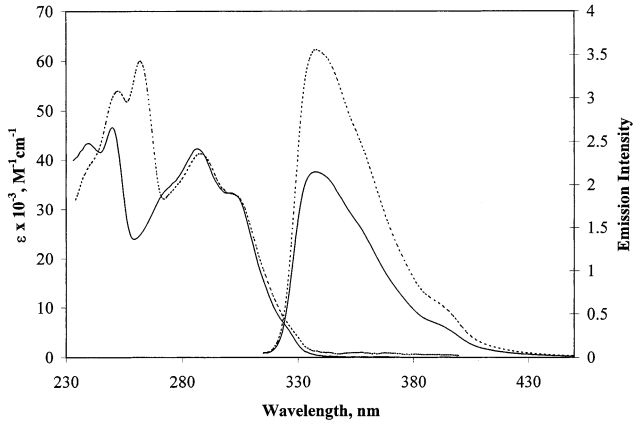

Fig. 10. Electronic absorption and emission spectra of ligands **46** (dashed line) and **47** (solid line) in deoxygenated CH_2Cl_2 solution. Reprinted, with permission, from Ref. [25].

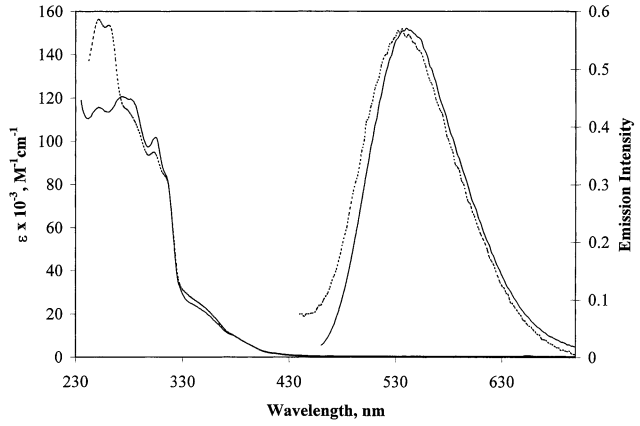

Fig. 11. Electronic absorption and emission spectra of complexes **48** (solid line) and **49** (dashed line) in deoxygenated CH_2Cl_2 solution. Reprinted, with permission, from Ref. [25].

precursor **42**, can be achieved using KOH in refluxing benzene. Precursor **43** was synthesized by selective coupling of **42** with 1-bromo-3-iodobenzene. Further coupling of **43** with trimethylsilylacetylene afforded precursor **44**. Deprotection of the trimethylsilyl group using KF in MeOH solution afforded precursor **45**. Precursor **45** was then used to synthesize cyclic ligands **46** and **47** using Sonogashira–Hagihara cross coupling and oxidative coupling with a Hay catalyst [114,115], respectively.

Dinuclear complexes **48** and **49** were prepared in a similar manner by refluxing the cyclic ligand and (t-Bu_2bpy)Re(CO)$_3$(CH_3CN)(PF_6) in THF (see Scheme 11) and subsequent recrystallization from CH_2Cl_2–hexane solution.

7.2. Photophysical properties

The obtained photophysical data, including absorption, emission spectral data, emission quantum yields

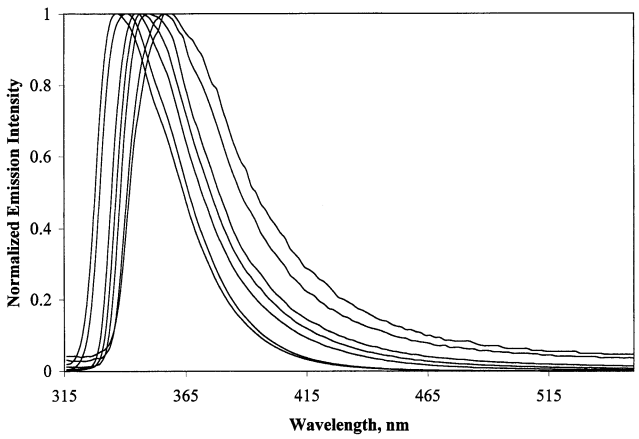

Fig. 12. Concentration dependent fluorescence spectra of cyclic ligand **46** in deoxygenated CH_2Cl_2. The spectra from left to right are recorded at concentrations of 1×10^{-5}, 1×10^{-4}, 1×10^{-3}, 2×10^{-3}, 4×10^{-3}, 8×10^{-3}, 1×10^{-2} M, respectively. Reprinted, with permission, from Ref. [25].

and lifetimes of complexes **48** and **49**, as well as ligands **46** and **47**, are summarized in Table 7. Figs. 10 and 11 present the absorption and emission spectra recorded from ligands **46** and **47** and complexes **48** and **49** in deoxygenated CH_2Cl_2 solution. The bands that appear below 320 nm for complexes **48** and **49** are assigned to the vibrational progression of π–π* absorptions, as evidenced from the similar vibrational structures in the corresponding ligands **46** and **47**. It is noted that, although the frameworks of ligands **46** and **47** are extended, the colors of **46** and **47** are only pale yellow because of the interruption of conjugation at the *meta*-connection [111]. The absorption bands that extend from 350 to 420 nm in complexes **48** and **49** are assigned to the combination of Re (dπ) to t-Bu_2bpy (ππ*) and Re (dπ) to cyclic ligand (π*) charge-transfer transitions.

Ligands **46** and **47** both exhibit strong blue fluorescence with similar band maxima and comparable lifetimes and quantum yields to each other. The emission data of complexes **48** and **49** in deoxygenated CH_2Cl_2 solution resemble one another in that each exhibits structureless bands and long lifetimes. The emissions are assigned to Re (dπ) to cyclic ligand (π*) charge-transfer transitions in the complexes. Ligand **46** exhibits concentration dependent fluorescence in CH_2Cl_2 solution (see Fig. 12). The fluorescence maximum shifts from 336 nm in 10^{-6} M solution to 358 nm in 10^{-2} M solution. There is no further spectral change observed below 10^{-6} M and precipitation occurs when the solution concentration is raised higher than 10^{-2} M. The fluorescence lifetime of **46** is best fitted to a biexponential decay (1.1 and 3.2 ns) when it is monitored at 460 nm where the emission comprises contributions from both monomer and excimer. The emission is best fitted as a single exponential decay (1.1 ns) when it is monitored at 320 nm where the emission is solely from the monomer.

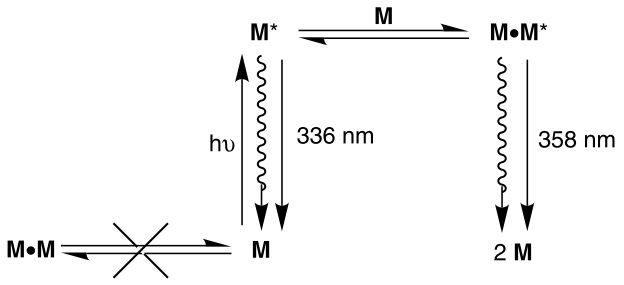

Scheme 12.

Cyclic ligand **47** exhibits a similar red shift in the fluorescence with the maximum moving from 336 nm at 10^{-6} M solution to 342 nm at $\sim 5 \times 10^{-4}$ M, which is near the point of saturation. The fluorescence decay of **47** also exhibits a biexponential process (1.1 and 3.6 ns) when it is monitored at 420 nm where the emission comprises contributions from both monomer and excimer. In contrast, the emission spectra and lifetimes are observed to be concentration independent for both complexes **48** and **49**.

Ligand **46** and complexes **48** and **49** do not exhibit any concentration dependence in the ^{1}H-NMR spectra recorded in CD_2Cl_2, ruling out the existence of any significant degree of ground state aggregation. We were unable to test the associative nature of ligand **47** by ^{1}H-NMR spectra due to the low solubility of this species. However, the lack of aggregation in solution of complexes **48** and **49** is thought to be due to the bulky *tert*-butyl groups which surely prevent close association. In ligand **46**, the electrostatic repulsion between the nitrogen atoms would seem to be responsible for the non-association behavior, as evidenced by the electrostatic potential plot based on an AM1 calculation. The same reasoning can also be applied to ligand **47** and it is, therefore, plausible to assume that there is no self-association for ligand **47** in solution either. Thus, the concentration dependent fluorescence bands observed in CH_2Cl_2 solution for ligands **46** and **47** cannot be attributed to ground state association.

Consequently, the concentration dependent fluorescence is best ascribed to an excited state aggregation process. Recently, Kopelman et al. have found the formation of excimers from some phenylacetylene dendrimers [116]. The excimer formation is observed in some solvents even at concentration as low as 7.0×10^{-8} M. The excimer emission is also observed for some poly(*p*-phenyleneethynylenes) polymers in solution [117]. We have also recently found some linear alkynyl bipyridines which exhibit concentration dependent excimeric emission [118]. Scheme 12 depicts the qualitative diagram of the excited state processes for ligands **46** or **47** and the lack of any ground state association. The biexponential decay of the emission at higher concentration for ligands **46** and **47** in CH_2Cl_2 confirms that there are indeed two distinct excited states present. The longer lifetime observed at the higher concentrations is, therefore, attributed to the excimer species.

8. Concluding remarks

We have demonstrated in this review that a variety of transition metal based supramolecular systems can be carefully designed to perform desired functionality such as molecular sensing and photoswitching. The large internal voids in self-assembly metallocyclophanes or cages discussed above render them to be potentially useful as molecular hosts for many different types of guest molecules. The incorporation of potential luminescent chromophores into the structures provides a very sensitive way to detect the presence of the guests. By judicious design of the polynuclear transition metal complexes, the energies of the excited states can be altered by external stimuli such as light or heat. Varying the order of the excited states facilitates these systems as potential molecular switches.

Acknowledgements

We are grateful to the Division of Chemical Sciences, Office of Basic Energy Sciences, Office of Science, US Department of energy (Grant DE-FG02-89ER14039), for funding the authors' research that is cited in this review.

References

[1] V. Balzani, A. Juris, M. Venturi, S. Campagna, S. Serroni, Chem. Rev. 96 (1996) 759.
[2] D.M. Roundhill, Photochemistry and Photophysics of Metal Complexes, Plenum Press, New York, 1994.
[3] A.J. Lees, Chem. Rev. 87 (1987) 711.
[4] V. Balzani, F. Scandola (Eds.),Supramolecular Photochemistry, Ellis Horwood, Chichester, UK, 1991.
[5] R.W. Balk, D.J. Stufkens, A. Oskam, Inorg. Chim. Acta 28 (1978) 133.
[6] R.W. Balk, D.J. Stufkens, A. Oskam, Inorg. Chem. 19 (1980) 3015.
[7] P.C. Servaas, H.K. van Dijk, T.L. Snoeck, D.J. Stufkens, A. Oskam, Inorg. Chem. 24 (1985) 4494.
[8] H.K. van Dijk, P.C. Servaas, D.J. Stufkens, A. Oskam, Inorg. Chim. Acta 104 (1985) 179.
[9] B.J. Holliday, C.A. Mirkin, Angew. Chem. Int. Ed. 40 (2001) 2022.
[10] M. Fujita, K. Umemoto, M. Yoshizawa, N. Fujita, T. Kusukawa, K. Biradha, Chem. Commun. (2001) 509.
[11] S. Leininger, B. Olenyuk, P.J. Stang, Chem. Rev. 100 (2000) 853.
[12] G.F. Swiegers, T.J. Malefetse, Chem. Rev. 100 (2000) 3483.
[13] D.L. Caulder, K.N. Raymond, J. Chem. Soc. Dalton Trans. (1999) 1185.

[14] L.R. MacGillivray, J.L. Atwood, Angew. Chem. Int. Ed. 38 (1999) 1018.
[15] M. Fujita, Chem. Soc. Rev. 27 (1998) 417.
[16] J. -M. Lehn, Supramolecular Chemistry, VCH Publishers, New York, 1995.
[17] R.V. Slone, K.D. Benkstein, S. Bélanger, J.T. Hupp, I.A. Guzei, A.L. Rheingold, Coord. Chem. Rev. 171 (1998) 221.
[18] S. -S. Sun, A.J. Lees, Inorg. Chem. 38 (1999) 4181.
[19] S.-S. Sun, A.J. Lees, J. Am. Chem. Soc. 122 (2000) 8956.
[20] S.-S. Sun, A.S. Silva, I.M. Brinn, A.J. Lees, Inorg. Chem. 39 (2000) 1344.
[21] S.-S. Sun, A.J. Lees, Inorg. Chem. 40 (2001) 3154.
[22] S.-S. Sun, A.J. Lees, Chem. Commun. (2001) 103.
[23] S.-S. Sun, E. Robson, N. Dunwoody, A.S. Silva, I.M. Brinn, A.J. Lees, Chem. Commun. (2000) 201.
[24] S.-S. Sun, A.J. Lees, Chem. Commun. (2000) 1687.
[25] S.-S. Sun, A.J. Lees, Organometallics 20 (2001) 2353.
[26] R.V. Slone, D.I. Yoon, R.M. Calhoun, J.T. Hupp, J. Am. Chem. Soc. 117 (1995) 11813.
[27] A.P. de Silva, H.Q.N. Gunaratne, T. Gunnlaugsson, A.J.M. Huxley, C.P. McCoy, J.T. Rademacher, T.E. Rice, Chem. Rev. 97 (1997) 1515.
[28] P.J. Giordano, M.S. Wrighton, J. Am. Chem. Soc. 101 (1979) 2888.
[29] R.W. Callahan, G.M. Brown, T.J. Meyer, Inorg. Chem. 19 (1980) 2797.
[30] J.V. Caspar, T.J. Meyer, J. Phys. Chem. 87 (1983) 952.
[31] A.I. Baba, J.R. Shaw, J.A. Simon, R.P. Thummel, R.H. Schmehl, Coord. Chem. Rev. 171 (1998) 43.
[32] V.W.-W. Yam, V.C.-Y. Lau, L.-X. Wu, J. Chem. Soc. Dalton Trans. (1998) 1461.
[33] A. Juris, S. Campagna, I. Bidd, J. -M. Lehn, R. Ziessel, Inorg. Chem. 27 (1988) 4007.
[34] K.D. Ley, Y. Li, J.V. Johnson, D.H. Powell, K.S. Schanze, Chem. Commun. (1999) 1749.
[35] K.D. Ley, K.S. Schanze, Coord. Chem. Rev. 171 (1998) 287.
[36] K.D. Ley, C.E. Whittle, M.D. Bartberger, K.S. Schanze, J. Am. Chem. Soc. 119 (1997) 3423.
[37] J.P. Desvergne, A.W. Czarnik (Eds.),Chemosensors of Ion and Molecule Recognition, Kluwer Academic Publishers, Boston, 1997.
[38] J.-S. Yang, T.M. Swager, J. Am. Chem. Soc. 120 (1998) 5321.
[39] S. Bélanger, M.H. Keefe, J.L. Welch, J.T. Hupp, Coord. Chem. Rev. 190–192 (1999) 19.
[40] M.H. Keefe, R.V. Slone, J.T. Hupp, K.F. Czaplewski, R.Q. Snurr, C.L. Stern, Langmuir 16 (2000) 3964.
[41] R.V. Slone, J.T. Hupp, C.L. Stern, T.E. Albrecht-Schmitt, Inorg. Chem. 35 (1996) 4096.
[42] S. Bélanger, J.T. Hupp, C.L. Stern, R.V. Slone, D.F. Watson, T.G. Carrell, J. Am. Chem. Soc. 121 (1999) 557.
[43] S. Bélanger, J.T. Hupp, C.L. Stern, Acta Crystallogr. C54 (1998) 1596.
[44] M.S. Wrighton, D.L. Morse, J. Am. Chem. Soc. 96 (1974) 998.
[45] A.J. Lees, Comments Inorg. Chem. 17 (1995) 319.
[46] E.C. Constable, M.D. Ward, Inorg. Chim. Acta 141 (1988) 201.
[47] E.C. Constable, A.M.W. Cargill Thompson, D.A. Tocher, M.A.M. Daniels, New J. Chem. 16 (1992) 855.
[48] E.C. Constable, A.M.W. Cargill Thompson, J. Chem. Soc. Dalton Trans. (1994) 1409.
[49] S. Campagna, G. Denti, L. Sabatino, S. Serroni, M. Ciano, V. Balzani, J. Chem. Soc. Chem. Commun. (1989) 1500.
[50] M.T. Indelli, F. Scandola, L. Flamigni, J.-P. Collin, J.-P. Sauvage, A. Sour, Inorg. Chem. 36 (1997) 4247.
[51] J.M. Calvert, J.V. Caspar, R.A. Binstead, T.D. Westmoreland, T.J. Meyer, J. Am. Chem. Soc. 104 (1982) 6620.
[52] E.J. Lee, M.S. Wrighton, J. Am. Chem. Soc. 113 (1991) 8562.
[53] J.-P. Sauvage, J.-C. Collin, S. Chambron, C. Guillerez, V. Coudret, V. Balzani, F. Barigelletti, L. De Cola, L. Flamigni, Chem. Rev. 94 (1994) 993.
[54] E.M. Kober, J.V. Caspar, R.S. Lumpkin, T.J. Meyer, J. Phys. Chem. 90 (1986) 3722.
[55] V. Grosshenny, A. Harriman, R. Ziessel, Angew. Chem. Int. Ed. Engl. 34 (1995) 1100.
[56] V. Grosshenny, A. Harriman, M. Hissler, R. Ziessel, J. Chem. Soc. Faraday Trans. 92 (1996) 2223.
[57] D.L. Dexter, J. Chem. Phys. 21 (1953) 836.
[58] T. Förster, Discuss. Faraday Soc. 27 (1959) 7.
[59] J.K.M. Sanders, Chem. Eur. J. 4 (1998) 1378.
[60] M. Fujita, N. Fujita, K. Ogura, K. Yamaguchi, Nature 400 (1999) 52.
[61] B. Olenyuk, J.A. Whiteford, A. Fechtenkötter, P.J. Stang, Nature 398 (1999) 796.
[62] M. Fujita, M. Aoyagi, F. Ibukuro, K. Ogura, K. Yamaguchi, J. Am. Chem. Soc. 120 (1998) 611.
[63] P.N.W. Baxter, J. -M. Lehn, B.O. Kneisel, D. Fenske, Angew. Chem. Int. Ed. Engl. 36 (1997) 1978.
[64] P.N.W. Baxter, J. Lehn, A. DeCian, Angew. Chem. Int. Ed. Engl. 32 (1993) 69.
[65] P.N.W. Baxter, J.-M. Lehn, B.O. Kneisel, G. Baum, D. Fenske, Chem. Eur. J. 5 (1999) 113.
[66] K.D. Benkstein, J.T. Hupp, C.L. Stern, Angew. Chem. Int. Ed. Engl. 39 (2000) 2891.
[67] K.D. Benkstein, J.T. Hupp, C.L. Stern, J. Am. Chem. Soc. 120 (1998) 12982.
[68] K.D. Benkstein, J.T. Hupp, Mol. Cryst. Liq. Cryst. 342 (2000) 151.
[69] A. Vogler, J. Kisslinger, Inorg. Chim. Acta 115 (1986) 193.
[70] M. Fujita, J. Yazaki, K. Ogura, Tetrahedron Lett. 32 (1991) 5589.
[71] H. Meier, Angew. Chem. Int. Ed. Engl. 31 (1992) 1399.
[72] H. Meier, Angew. Chem. Int. Ed. 40 (2001) 1851.
[73] H. Gorner, H.J. Kuhn, Adv. Photochem. 19 (1995) 1.
[74] K. Sandros, M. Sundahl, O. Wennerstrom, U. Norinder, J. Am. Chem. Soc. 112 (1990) 3082.
[75] J. Saltiel, G.R. Marchand, E. Kirkor-Kaminska, W.K. Smothers, J.L. Charlton, W.B. Mueller, J. Am. Chem. Soc. 106 (1984) 3144.
[76] K.S. Schanze, L.A. Lucia, M. Cooper, K.A. Walters, H.-F. Ji, O. Sabina, J. Phys. Chem. A 102 (1998) 5577.
[77] J.R. Shaw, R.H. Schmehl, J. Am. Chem. Soc. 113 (1990) 389.
[78] M.S. Wrighton, D.L. Morse, J. Am. Chem. Soc. 96 (1974) 998.
[79] P.P. Zarnegar, C.R. Bock, D.G. Whitten, J. Am. Chem. Soc. 95 (1973) 4367.
[80] J.D. Lewis, R.N. Perutz, J.N. Moore, Chem. Commun. (2000) 1865.
[81] J.T. Lin, S.-S. Sun, J.R. Wu, Y.C. Liaw, K.-J. Lin, J. Organomet. Chem. 517 (1996) 27.
[82] G. Tapolsky, R. Duesing, T.J. Meyer, Inorg. Chem. 29 (1990) 2285.
[83] P.D. Beer, D.K. Smith, Prog. Inorg. Chem. 46 (1997) 1.
[84] F.P. Schmidtchen, M. Berger, Chem. Rev. 97 (1997) 1609.
[85] P.D. Beer, P.A. Gale, Angew. Chem. Int. Ed. Engl. 40 (2001) 486.
[86] L. Fabbrizzi, M. Licchelli, G. Rabaioli, A. Taglietti, Coord. Chem. Rev. 205 (2000) 85.
[87] P.D. Beer, J. Cadman, Coord. Chem. Rev. 205 (2000) 131.
[88] M.H. Keefe, K.D. Benkstein, J.T. Hupp, Coord. Chem. Rev. 205 (2000) 201.
[89] P.A. Gale, P. Anzenbacher, J.L. Sessler, Coord. Chem. Rev. 222 (2001) 57.
[90] L.J. Prins, D.N. Reinhoudt, P. Timmerman, Angew. Chem. Int. Ed. Engl. 40 (2001) 2382.

[91] C.R. Cooper, N. Spencer, T.D. James, Chem. Commun. (1998) 1365.
[92] C.B. Black, B. Andrioletti, A.C. Try, C. Ruiperez, J.L. Sessler, J. Am. Chem. Soc. 121 (1999) 10438.
[93] A.P. Bisson, V.M. Lynch, M.-K.C. Monahan, E.V. Anslyn, Angew. Chem. Int. Ed. Engl. 36 (1997) 2340.
[94] C.A. Hunter, L.D. Sarson, Angew. Chem. Int. Ed. Engl. 33 (1994) 2313.
[95] K.-S. Jeong, Y.L. Cho, J.U. Song, H.-Y. Chang, M.-G. Choi, J. Am. Chem. Soc. 120 (1998) 10982.
[96] K. Kavallieratos, S.R. de Gala, D.J. Austin, R.H. Crabtree, J. Am. Chem. Soc. 119 (1997) 2325.
[97] K.A. Connors, Binding Constants, firsst ed., Wiley, New York, 1987.
[98] D.E. Kaufmann, A. Otten, Angew. Chem. Int. Ed. Engl. 33 (1994) 1832.
[99] D.A. Bell, E.V. Anslyn, in: J.L. Atwood, J.E.D. Davies, D.D. MacNicol, F. Vogtle, J.-M. Lehn (Eds.), Comprehensive Supramolecular Chemistry, vol. 2 (chapter 14), Pergamon, Oxford, 1996.
[100] P. Tecilla, S.-K. Chang, A.D. Hamilton, J. Am. Chem. Soc. 112 (1990) 9586.
[101] K. Kavallieratos, R.H. Crabtree, Chem. Commun. (1999) 2109.
[102] F. de Jong, H.C. Visser, in: J.L. Atwood, J.E.D. Davies, D.D. MacNicol, F. Vogtle, J.-M. Lehn (Eds.), Comprehensive Supramolecular Chemistry, vol. 10 (chapter 2), Pergamon, Oxford, 1996.
[103] L.A.J. Chrisstoffels, F. de Jong, D.N. Reinhoudt, Chem. Eur. J. 6 (2000) 1376.
[104] J.S. Moore, Acc. Chem. Res. 30 (1997) 402.
[105] M.M. Haley, J.J. Pak, S.C. Brand, Top. Curr. Chem. 201 (1999) 81.
[106] P.-H. Ge, W. Fu, W.A. Herrmann, E. Herdtweck, C. Campana, R.D. Adams, U.H.F. Bunz, Angew. Chem. Int. Ed. 39 (2000) 3607.
[107] O.Y. Mindyuk, M.R. Stetzer, P.A. Heiney, J.C. Nelson, J.S. Moore, Adv. Mater. 10 (1998) 1636.
[108] D. Venkataraman, S. Lee, J.S. Moore, Nature 371 (1994) 591.
[109] Y. Tobe, N. Utsumi, A. Nagano, K. Naemura, Angew. Chem. Int. Ed. Engl. 37 (1998) 1285.
[110] H.L. Anderson, A. Bashall, K. Hendrick, M. Mcpartlin, J.K.M. Sanders, Angew. Chem. Int. Ed. Engl. 33 (1994) 429.
[111] D.L. Morrison, S. Höger, Chem. Commun. (1996) 2313.
[112] K. Sonogashira, Y. Tohda, N. Hagihara, Tetrahedron Lett. 16 (1975) 4467.
[113] S.N. Takahashi, Y. Kuroyama, K. Sonogashira, N. Hagihara, Synthesis (1980) 627.
[114] A.S. Hay, J. Org. Chem. 27 (1962) 3320.
[115] S. Höger, A.-D. Meckenstock, S. Müller, Chem. Eur. J. 4 (1998) 2423.
[116] S.F. Swallen, Z. Zhu, J.S. Moore, R. Kopelman, J. Phys. Chem. B 104 (2000) 3988.
[117] H. Li, D.R. Powell, R.K. Hayashi, R. West, Macromolecules 31 (1998) 52.
[118] S.-S. Sun, A.J. Lees, J. Photochem. Photobiol. A 140 (2001) 157.